(2)

ARMY RESEARCH LABORATORY

Formulation of a Next-Generation Interior Ballistic Code

Paul S. Gough

ARL-CR-68 October 1993

prepared by

Paul Gough Associates, Inc.
1048 South St.
Portsmouth, NH 03801-5423

under contract

DAAA15-91-M-0073

93

4

NOTICES

Destroy this report when it is no longer needed. DO NOT return it to the originator.

Additional copies of this report may be obtained from the National Technical Information Service, U.S. Department of Commerce, 5285 Port Royal Road, Springfield, VA 22161.

The findings of this report are not to be construed as an official Department of the Army position, unless so designated by other authorized documents.

The use of trade names or manufacturers' names in this report does not constitute indorsement of any commercial product.

REPORT DOCUMENTATION PAGE

Form Approved
OMB No 0704-0188

1. AGENCY USE ONLY (Leave blank)	2. REPORT DATE	3. REPORT TYPE AND DATES COVERED
	October 1993	Final, May 91 - Dec 91

4. TITLE AND SUBTITLE

Formulation of a Next-Generation Interior Ballistic Code

5. FUNDING NUMBERS

PR: 1L161102AH43
CC: DAAA15-91-M-0073

6. AUTHOR(S)

Paul S. Gough

7. PERFORMING ORGANIZATION NAME(S) AND ADDRESS(ES)

Paul Gough Associates, Inc.
1048 South St.
Portsmouth, NH 03801-5423

8. PERFORMING ORGANIZATION REPORT NUMBER

PGA-TR-91-3

9. SPONSORING / MONITORING AGENCY NAME(S) AND ADDRESS(ES)

U.S. Army Research Laboratory
ATTN: AMSRL-OP-CI-B (Tech Lib)
Aberdeen Proving Ground, MD 21005-5066

10. SPONSORING / MONITORING AGENCY REPORT NUMBER

ARL-CR-68

11. SUPPLEMENTARY NOTES

Point of Contact for this report is Dr. George E. Keller, U.S. Army Research Laboratory, ATTN: AMSRL-WT-PE, Aberdeen Proving Ground, MD 21005-5066.

12a. DISTRIBUTION AVAILABILITY STATEMENT

Approved for public release; distribution unlimited.

12b. DISTRIBUTION CODE

13. ABSTRACT (Maximum 200 words)

Two-phase flow interior ballistic codes, both one-dimensional and two-dimensional, have been developed over the last 20 years for the purpose of modeling the behavior of solid propellant gun propulsion systems. These codes have proven useful for explaining charge malfunctions and for studying possible remedies. Over the years, these codes have become increasingly elaborate as more complex designs have been addressed and also as the depth of simulation has increased. However, charge designs involving liquid propellant or electrothermal-chemical propulsion remain largely outside the scope of the solid propellant codes and a number of separate codes have been developed for the simulation of these alternative propulsion schemes.

As we look to the future, it is evident that the next generation of interior ballistic models will be required to address three-dimensional details of the flow inside the gun. Such models will be expensive to develop and it is, therefore, of great interest to assess the extent to which a single code can be formulated to treat all foreseeable propulsion schemes.

In this report, we review the physical problems of current interest, as well as those anticipated in the foreseeable future. We review the models currently available to address these processes. We then discuss the architecture of a possible next-generation code. This discussion addresses the formulation of the equations, the choice of solution algorithms, and the implications of the current trend toward massively parallel computing.

14. SUBJECT TERMS	15. NUMBER OF PAGES
two dimensional flow, one dimensional flow, electrothermal-chemical propulsion, interior ballistic modeling, interior ballistics	67
	16. PRICE CODE

17. SECURITY CLASSIFICATION OF REPORT	18. SECURITY CLASSIFICATION OF THIS PAGE	19. SECURITY CLASSIFICATION OF ABSTRACT	20. LIMITATION OF ABSTRACT
UNCLASSIFIED	UNCLASSIFIED	UNCLASSIFIED	UL

INTENTIONALLY LEFT BLANK.

PREFACE

Technical cognizance for the subject U.S. Army Research Laboratory contract was provided by Dr. George E. Keller, Weapons Technology Directorate, Propulsion and Flight Division, Propulsion Physics Branch.

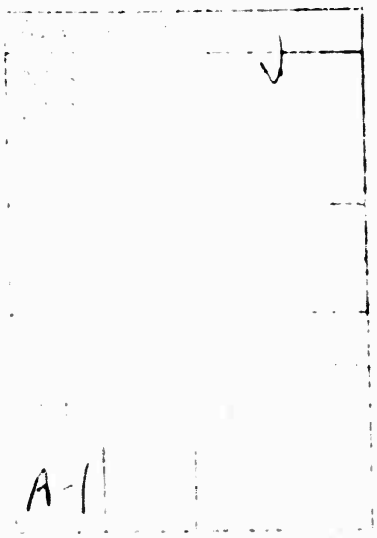

INTENTIONALLY LEFT BLANK.

ACKNOWLEDGMENT

The author acknowledges with gratitude the guidance and advice provided by Dr. Elaine Oran in regard to the use of Flux-Corrected Transport.

INTENTIONALLY LEFT BLANK.

TABLE OF CONTENTS

INTENTIONALLY LEFT BLANK.

LIST OF FIGURES

INTENTIONALLY LEFT BLANK.

1. INTRODUCTION

There are many aspects to propelling charge design. The central problem, as it is called by Corner [1], is the determination of the maximum pressure in the gun and the muzzle velocity of the projectile. But other issues of great importance include: (a) the heat transfer to the tube which controls thermal erosion, or the rate of wear, as well as the safe rate of fire; (b) movable and/or permeable boundaries added to the standard long-tube chamber configuration; and (c) the blast and possible secondary combustion processes which occur after the projectile leaves the gun and which impact both safety and exposure to detection. The focus here is on the central problem extended to mean the determination of the distributed pressure field in a gun as influenced by minute details of the distribution of energy release. In particular, we are interested in the degree to which all presently considered gun propulsion schemes can be modeled in three-dimensional detail by a single code. Such a code would necessarily subsume all the capabilities of the several codes presently used to model a variety of propulsion schemes and is referred to as a next-generation code. While the focus is on the central problem, we will comment on the relevance of such a code in the general area of heat transfer. We will also note instances in which existing codes have capabilities relative to the simulation of muzzle blast.

It was recognized quite early by experimentalists that the pressure field in a gun chamber could exhibit oscillations or wave structure [2,3]. Moreover, the influence of the distribution of the propellant and its manner of ignition was appreciated by these pioneers. However, whereas Hedden and Nance [3] argued that the presence of pressure waves was essentially benign, the review by Budka and Knapton [4] emphasized the pervasiveness with which gun charge malfunctions were associated with the presence of such waves. The question of the acceptability of pressure waves in solid propellant guns is discussed in some detail by May and Horst [5] who also examine the relationship between various details of charge design and the formation of such waves.

The earliest digital simulations of gun interior ballistics were based on a lumped-parameter formulation and, therefore, were unable to analyze the structure of the pressure field and the influence of charge configuration [6]. Nevertheless, such codes are of great utility and remain in widespread use today more than 30 years after their initial development. By the early 1970s, interest developed in the formulation of one-dimensional two-phase flow models of solid-phase interior ballistics. A variety of stimuli combined

with the availability of increased computer resources to precipitate the formulation of several codes [7,8,9,10]. The code written by Gough and Zwarts [8] has remained under continuous development through the present date and is now applicable to a wide variety of solid propellant configurations [11].

The last 20 years have seen increased attention to alternatives to solid propellants. Liquid propellants have long been of interest because of their low cost and logistical advantages [12]. More recently, interest has developed in electrothermal guns in which an external energy supply circumvents the energy density limitations inherent in chemical propellants [13]. These alternative concepts have resulted in the development of many codes of varying levels of sophistication.

The situation today is such that separate codes are used to analyze different types of propulsion schemes. Two-dimensional capabilities exist for the modeling of many designs and, in some cases, three-dimensional schemes are available. But no single code is able to address all types of gun propulsion systems and limitations exist even in respect to the specific categories addressed by certain of the codes. In this report, we review the various types of propulsion systems which are of current interest. We discuss the current modeling capability with respect to each of them. We then identify a system of equations capable of treating all the configurations in a unified model and discuss an appropriate method of solution.

Present-day two-dimensional simulations of gun propelling charges of all types require about 1 hour of CPU time on a CRAY supercomputer. Three-dimensional calculations may be expected to require one to two orders of magnitude more computer resources. Further demands may be imposed if complex chemical schemes are to be modeled. At the present time, it is likely that gains of two to three orders of magnitude in computer speed will only be obtained with massively parallel computer architectures. Accordingly, our discussion of the next-generation code reflects the implications of such emerging systems insofar as the choice of solution algorithm is concerned.

2. PROPELLING CHARGE CONFIGURATIONS

Figure 1 illustrates a bag charge of granular propellant for the 155-mm howitzer. The charge consists of a number of randomly packed grains whose individual shapes are regular and precisely formed. The charge shown contains about 1,000 such grains each of which is a right circular cylinder containing seven perforations. The grains are packed around a nitrocellulose tube. The tube contains a centercore of black powder which is an important element of the ignition train. The charge is contained in a cloth bag which

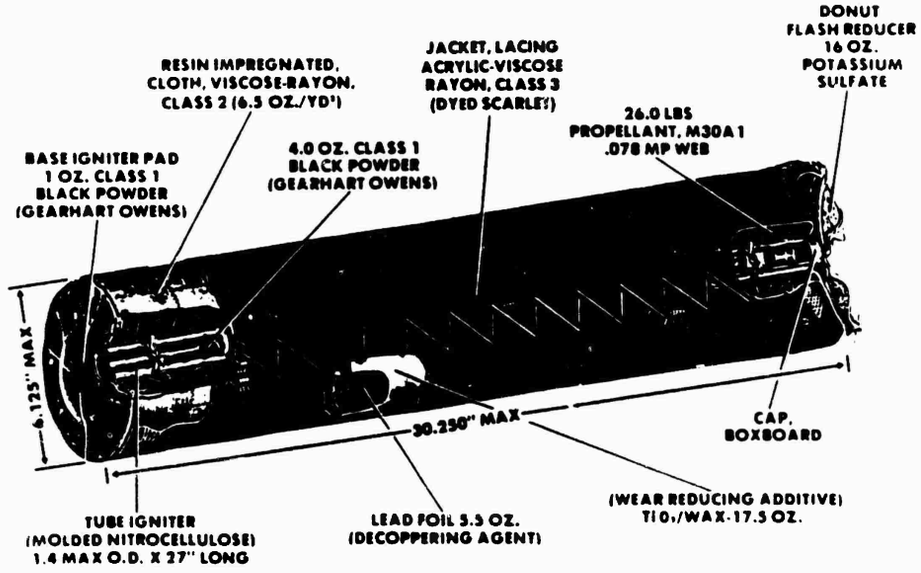

Figure 1. Solid propellant bagged charge.

embeds other system components. A basepad igniter is attached at the rear. A bag of flash suppressant is attached at the front. Wear-reducing additives and a lead foil decoppering agent are embedded in the forward part of the exterior. The charge is, therefore, initially confined in a container whose surface properties, particularly permeability, vary from point to point. The charge is subcaliber and, when loaded, sits on the bottom surface of the tube. Ullage is present behind the charge, in front of it and around it. The initial configuration is clearly three-dimensional, although not strongly so.

The basepad is ignited by a discharge from a spithole in the breech. The combustion products of the basepad are intended to flow into the centercore which, ideally, should then ignite over its length. Subsequently, the ideal situation involves the axially uniform ignition of the main charge by the radial convection of the centercore combustion products. In practice this goal is not realized. The combustion products of the basepad may partially penetrate the bag and ignite the main charge independently of the centerline stimulus. Combustion products are also free to flow through the ullage at the rear of the charge, thence around the charge, and possibly into the forward region of ullage. Depending on the permeability of the bag, these combustion products may induce ignition in any number of ways. Evidently, there is a strong coupling of the details of ullage distribution, igniter stimulus, and container properties.

Figure 2 illustrates a second type of artillery charge. The unicharge represents an approach to covering all firing zones with varying numbers of identical increments, one of which is illustrated in the figure. In contrast to the bag charge, the unicharge increment is contained in a relatively stiff container whose structural properties may influence the path of flamespreading. Moreover, as we have noted, several such increments will normally be present.

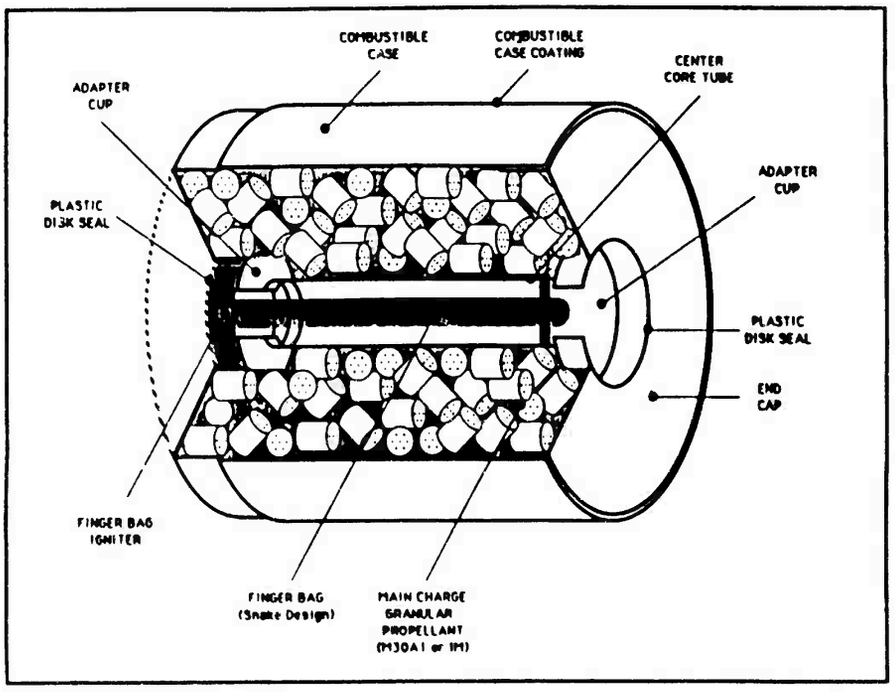

Figure 2. Solid propellant unicharge increment.

Figure 3 illustrates two types of propelling charges that are under current consideration for the 120-mm tank gun. In both cases, we note the presence of a combustible cartridge case, which conforms to the tube; and a projectile afterbody, which extends into the combustion chamber. The afterbody also has fins which contribute three-dimensional details to the configuration. We also note, in both cases, the presence of an interface between the increments. The first design consists of two increments of slotted stick propellant; the second, of granular propellant. A stick propellant bed is clearly different from a granular charge in that its structure is more regular. Axial permeability is high. The sticks considered in this case have a central perforation. The slot allows gas, due to combustion in the perforation, to flow freely to the exterior of the grains. It should be noted, however, that some stick charges are unslotted.

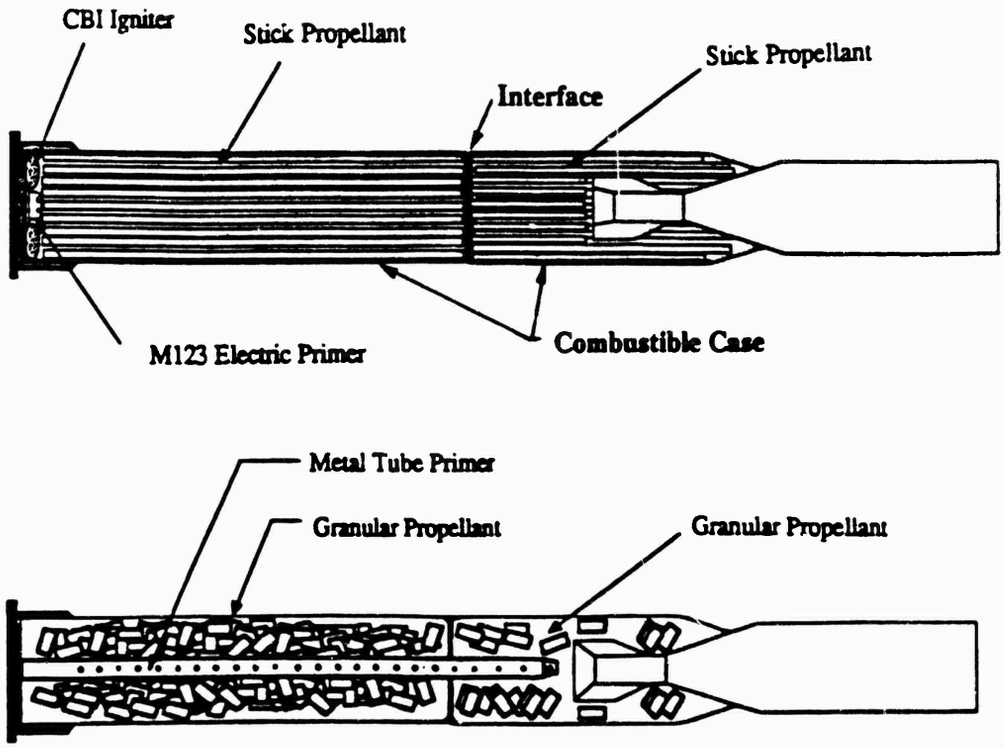

Figure 3. Two solid-propellant cartridge configurations for a tank gun.

In such charges, combustion in the perforations can proceed at a different rate from that on the exterior surfaces. The flow in the perforations is coupled to that in the exterior only at the ends of the sticks. In some cases, the efflux from the perforations can choke, at which point the interior flow becomes independent of the exterior. Pressure differences can lead to rupture of the sticks.

Figure 4 illustrates a completely different propulsion scheme, namely, a current design of a Regenerative Liquid Propellant Gun (RLPG). In this system, an injection piston moves rearward relative to a control piston which is also mobile. The relative motion causes liquid propellant in the reservoir to be injected in the form of a jet into the combustion chamber. Although the pressure in the reservoir must necessarily exceed that in the combustion chamber, rearward motion of the injection piston is assured by a differential in the surface area exposed on either side.

The mechanical complexity of the RLPG represents an engineering tradeoff which allows control over the combustion rate of the liquid propellant to a degree comparable to that obtained with the geometrically regular solid propellant grains. In spite of the mechanical compensation, the combustion processes in the RLPG remain dependent on the details of the disintegration of the jet of injected propellant. High-frequency oscillations have been observed in the pressure histories of such designs.

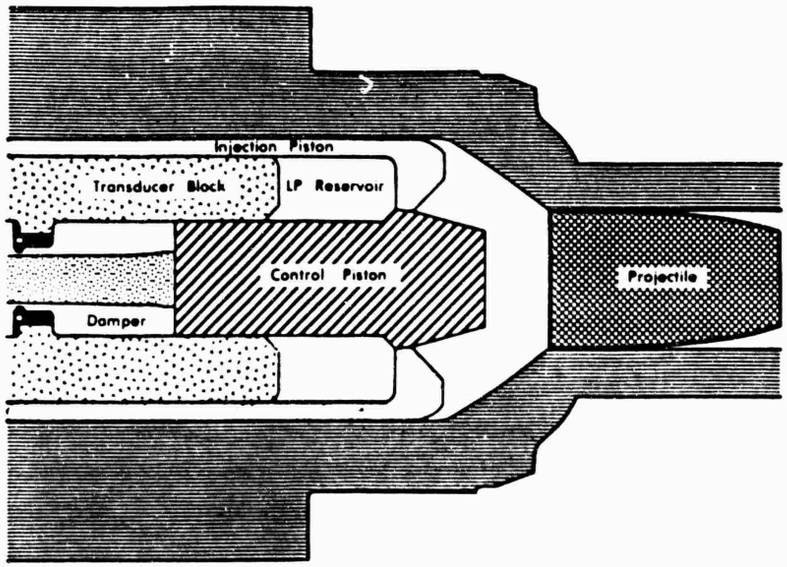

Figure 4. A regenerative liquid propellant gun design.

Although Figure 4 illustrates an axisymmetric configuration, three-dimensional details may be introduced by sidewall injection of igniter products as well as the presence of mechanical components in the combustion chamber. Figure 5 illustrates, schematically, yet another propulsion system of current interest, the electrothermal (ET) gun. In this system, the energy is supplied by an external energy supply which creates an intensely heated plasma. The plasma flows into a working fluid which is pressurized by the heat addition and which provides the propulsive force to the projectile. At present, this ideal concept is not thought to be practical and variants are under study in which the plasma provides only part of the energy and the balance is provided by an exothermic working fluid. The working fluid may be homogeneous or it may be a bi-propellant. This extended concept, referred to as the electrothermal chemical gun (ETCG), subsumes the earlier bulk-loaded liquid propellant gun (BLPG) system. Whereas control of the pressure in the ideal ET system is clearly provided by the rate of delivery of electrical energy, that of the ETCG depends on the complex, turbulent mixing processes in a degree proportional to the fraction of energy which is delivered chemically. Depending on the plasma delivery system, processes in the ETCG may be either axisymmetric or three-dimensional.

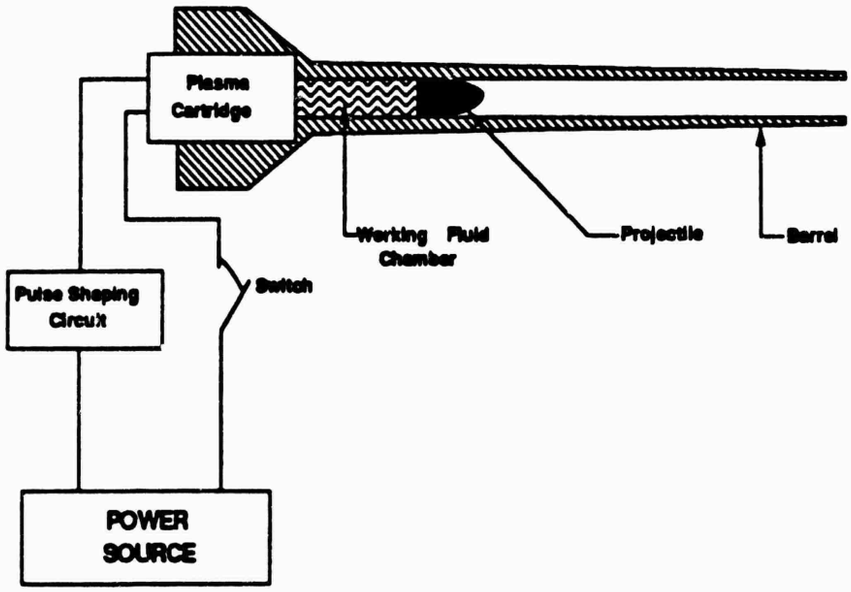

Figure 5. Schematic of an ET gun system.

The foregoing review of disparate propulsion schemes is by no means exhaustive. Notable omissions include: the monolithic charge, a single, homogeneous grain of rapidly burning propellant which may include arbitrary degrees of three-dimensional structure; traveling charges, which are attached to the projectile base and burn only on the rear surface; in-bore rockets; in-bore ramjets; liquid propellant traveling charges; and, finally, hybrid systems which comprise any combination of the foregoing schemes.

3. CURRENT COMPUTER CODES

We discuss the models in a sequence which corresponds to the discussion of propelling charges in the previous section.

3.1 Solid Propellant Charges. We have already mentioned a number of lumped parameter and one-dimensional codes which address this class of propelling charges. Models to treat two-dimensional details of the solid propellant charges have been presented by Gough [14], Meineke and Heiser [15], Groenenboom and Thomsen [16], Fitt et al. [17], Gibeling and McDonald [18], and by Schmitt [19]. All of these codes are based on a macroscopic formulation in which average properties of the two-phase flow constitute the modeled field variables. The porosity, or void fraction, is formally introduced by the averaging process. The equations require empirical resolution of constitutive laws to describe such microprocesses as interphase drag, heat transfer, and combustion.

The code developed by Gough [14] is referred to as TDNOVA. The TDNOVA Code is based on an explicit two-step finite difference scheme applied to the two-dimensional equations for macroscopic two-phase flow. The finite difference solver is a modified version of the MacCormack scheme [20] with boundary values determined using characteristic forms. The code was developed for the specific purpose of analyzing the interactions between the ignition train, the charge container properties, and the distribution of ullage in artillery charges. Accordingly, careful attention is paid to the location of the internal boundaries defined by the boundaries of the charge increments. The breechface and the tube walls are taken to be rigid, impermeable boundaries, while the base of the projectile constitutes a moving, impermeable boundary. The computational domain defined by these boundaries is divided into subregions which are linked by explicit boundary conditions. The boundary conditions which apply at interfaces between the propellant and the ullage consist of finite balances of mass, momentum, and energy. These are utilized to represent the presence of the container which is, therefore, idealized as a surface attribute of the region occupied by the propellant increment. The gas-phase boundary conditions capture the flow resistance and reactivity of the container at each location. Rupture of the container is modeled and is the mechanism whereby the surface flow resistance may decrease to zero. The centercore igniter is also modeled and is represented as a one-dimensional two-phase flow.

The code models a wide variety of conventional propellant granulations, including stick propellants. Anisotropic constitutive laws apply in the case of sticks. Perforated sticks, both slotted and unslotted, are modeled and are given a dual-voidage representation in which the flow in the interstices is distinguished from that in the perforations. A single global gas-phase chemical reaction is modeled to treat situations in which the energy release by the propellant is slow.

The code has been applied to a number of artillery charge configurations [21,22] However, the current mesh algorithm is not well suited to tank gun charges in which a long afterbody is present. Combustible cartridge cases are not modeled. While several increments may be present, these must be packaged end-to-end and not concentrically The mesh algorithm requires that the diameter of one increment not differ too much from that of its neighbor. Viscous or diffusive effects are not considered in the mixture regions. Normally, the ullage is represented as a number of one-dimensional regions linked at the increment corners by lumped parameter regions. Coding has been included to represent the flow in the ullage according to a Navier-Stokes formulation, but only partial solutions have been reported to date [23].

The codes developed by Meineke and Heiser [15] and by Fitt et al. [17] are also based on explicit finite difference solvers. These codes do not treat the propellant increment boundaries as explicit discontinuities, nor is there any representation of the container. Accordingly, they may be viewed as subject to more stringent limitations than TDNOVA.

The codes described by Gibeling [18] and by Schmitt [19] represent an extension relative to TDNOVA in one respect. These codes are based on an implicit solution of the two-phase equations with the addition of viscous and heat conduction terms. The goal of these codes was the determination of the tube wall boundary layer fully coupled to the combustion of the propellant. However, no explicit internal boundaries were considered and no attention was given to the presence of the container. The solution was based on the Linearized Alternating Direction Scheme of Briley and McDonald [24]. Complete solutions were presented only for single-phase flows and dilute mixtures of non-reacting spheres.

The final code of interest here is that described by Groenenboom and Thomsen [16] and is referred to as the PISCES Code [25]. PISCES is a proprietary, multi-purpose code capable of treating complicated structures coupled to fluid systems. PISCES contains several types of simulation modules. The basic set comprises an Euler solver, a Lagrange solver, a thin shell solver, and a rigid body solver. The equations addressed by the Euler solver are the Navier-Stokes equations for a non-reacting, single-component flow. Turbulence can be modeled according to a mixing-length theory or an algebraic law. Also, the stress deviator allows for material strength. These equations are solved according to an explicit finite-volume method based on the second-order upwind scheme of van Leer [26,27].

The computational domain is broken up into regions where each is covered with a structured grid. Coupling of the regions to one another and to the regions associated with the Lagrange thin shell, and rigid body solvers is accomplished by allowing boundary conditions to be imposed on any face of any cell. Moreover, cells are classified as open, covered, or partially covered. Covered cells are not updated. Partially covered cells arise from the overlap of a structural element with a computational cell for the fluid. For such a cell, the finite volume analysis is applied only to the uncovered fraction and the boundary conditions which couple the flow to the structure are, therefore, applied within the cell.

To treat solid propellant charges, an additional flow solver was developed [28]. The governing equations are the balance equations for macroscopic two-phase flow and conform with those used in references 14-17. They are solved using an explicit, finite volume, donor-cell scheme for the advection terms and a locally implicit scheme for the source and phase interaction terms.

The charge increment boundary is not considered to be an explicit discontinuity and no provision is made for the representation of the container. However, it would seem that the PISCES code could accommodate at least a partial representation of the container by treating it as a thin shell. Extensions would be required to describe the rupture, permeability, and reactivity of the container. We note that the choice of donor-cell differencing, while stable, can be very diffusive [29]. Therefore, thin regions of ullage around an increment would likely be contaminated by diffusion from the mixture. Given the physical importance of relatively small regions of ullage in respect to the path of flamespreading, this is a serious concern. Possibly, a flux-limiting method [29] would improve the situation.

3.2 Regenerative Liquid Propellant Gun. A number of lumped parameter and one-dimensional codes have been written to model the complete interior ballistic history of the RLPG [30-33]. Two-dimensional, two-phase analyses have been reported by Heiser [34] and by Steffens et al. [35]. The formulation of the equations was essentially the same as that used in the previously discussed solid-phase analyses. In fact, Heiser used the code described in reference 15 as a starting point. The solution was obtained using the explicit MacCormack scheme [20]. Heiser solved the two-dimensional equations only in the combustion chamber and the tube. The liquid reservoir was modeled as lumped parameter and the rate of injection of propellant followed from an unsteady formulation of the Bernouilli equation. Jet breakup was not considered. The injected propellant was assumed to decompose instantaneously into spherical droplets whose diameter was determined by a critical value of the Weber number based on the relative velocity of the phases. Steffens et al. [35] likewise solved the two-dimensional, two-phase equations in the combustion chamber and the tube. However, a two-dimensional analysis was also made of the flow in the reservoir. The PISCES Code was used to model both the flow and the moving mechanical elements of the RLPG. Injection was assumed to follow from the unsteady Bernouilli equation using boundary values of the pressure on each side of the piston. Like Heiser, Steffens et al. assumed instantaneous jet breakup and determined the droplet size from a Weber number criterion.

More recently, Steffens et al. [36] have reported simulations of aspects of RLPG behavior using the three-dimensional capability of the PISCES Code. Topics considered included the collapse of a bubble in the propellant reservoir, injection of propellant into the chamber, and transverse injection of igniter gas into the chamber. The paper also shows an application to the analysis of the flow around a muzzle brake.

Recent work by Coffee [37] has been based on an explicit finite volume solution of the two-dimensional Navier-Stokes equations for a homogeneous mixture of gas and droplets in the combustion

chamber and gun tube. The propellant jet is not modeled. The influx is predetermined from a lumped parameter analysis and is expressed as a boundary condition over part of the piston face. The application of this analysis has been focused on the structure of pressure oscillations rather than on predicting the overall ballistic behavior.

3.3 Electrothermal-Chemical Guns. As we have discussed previously, the phenomenology of this class of propulsion schemes is similar in many respects to that of the BLPG. In fact, Kuo et al. have proposed the use of the same two-dimensional model to treat both types [38,39]. Two-dimensional models have also been discussed by Kashiwa et al. [40], Cook et al. [41], Winsor et al. [42], Sinha et al. [43], and Hsiao et al. [44]. These models all differ as to the number of processes taken into consideration.

The model described by Chen [39] focuses on the events in the combustion chamber and gun tube with the plasma formation embedded into a boundary condition. The flow in the chamber is represented as one in which a central Taylor cavity progressively penetrates the working fluid which may be chemically reactive. The flow in the cavity is represented by the two-dimensional equations for macroscopic two-phase flow with the effects of viscosity and heat conduction included. The gas-phase is considered to be a multicomponent mixture and the condensed-phase is an aggregate of droplets. Droplets are formed on the surface of the Taylor cavity according to an empirical correlation. Turbulence is modeled according to a k-ε formulation. The complete model treats the outer region, which is occupied by undecomposed working fluid, as a two-dimensional flow. Detailed boundary conditions link the outer and inner flows. Solutions were obtained subject to simplifying assumptions. In particular, it was assumed that the cavity remained cylindrical at all times and continuum analysis could therefore be confined to the cavity. The implicit SIMPLE scheme of Patanker and Spalding [45] was used to obtain the numerical solution of the reduced set of model equations.

The model of Kashiwa et al. [40] includes details of the rate of plasma formation which is analyzed according to a lumped parameter formulation. The flow in the gun chamber and tube is described by the equations for a turbulent, chemically-reacting multispecies fluid with a single velocity and temperature at each point. Unlike the representation of Chen [39], the flow is viewed as locally homogeneous and no internal Taylor cavity boundary is considered. A semi-implicit, total variation diminishing, finite volume method is used to solve the balance equations.

The model of Cook et al. [41] has a physical basis intermediate to those of Kashiwa [40] and Chen [39]. A one-dimensional model describes the formation of the plasma in the capillary. The chamber and tube are viewed as containing a multicomponent, multiphase mixture which is represented as two-dimensional. The effects of diffusion are retained, turbulence being modeled according to a mixing length analysis. The balance equations are solved using the implicit ADI method of Peaceman and Rachford [46].

The model of Winsor [42] focuses on the flow in the combustion chamber and the tube. A finite element approach is used with an adaptive unstructured grid to obtain solutions to the Navier-Stokes equations subject to an arbitrary equation of state. Turbulence and multiphase effects are not considered. To capture shocks and other discontinuities, the solution incorporates the principle of flux-corrected transport (FCT) [29] in the manner described by Löhner et al. [47].

The work of Sinha et al. [43] also addresses the flow in the combustion chamber. A multidimensional solver is provided for the Navier-Stokes equations with detailed chemistry and turbulence models. The solution technique is based upon an implicit finite volume formulation with upwind differencing according to the methodology of Roe. A solver to treat clouds of particulates according to the same principles is also described.

The final model considered here is that of Hsiao et al. [44]. This model treats both the plasma formation and the flow in the combustion chamber. Fourth Order FCT analysis is applied to solve the balance equations in the combustion chamber. These are multidimensional formulations of the equations for a multicomponent, multiphase mixture with detailed chemical reaction and turbulence laws.

4. NEXT-GENERATION CODE

It is clear that a code capable of treating the types of gun propulsion systems considered here must be based on a solution of the balance equations for a multiphase, turbulent reacting flow. The admissible boundary conditions must be of the most general type. A modular coding structure is desired in which a central flow solver is supported by separate routines which express the constitutive laws. Such an approach facilitates the addition, modification, or replacement of the models used to define the equations of state, the interphase processes, the structure of turbulence, and the chemical interactions.

This section of the report contains two subsections. In the first, we present the balance equations which must be addressed by the central flow solver. We discuss the relationship of these equations to those used to model each of the types of propelling charges in the current codes. We also discuss the nature of the constitutive laws required to close the system of governing equations. Finally, we comment on the boundary conditions. This last topic includes some discussion of the modeling of the tube, the projectile, and the properties of the increment container.

The second subsection addresses the method of solution. It will be seen that we favor the use of the explicit FCT algorithm described by Oran [29]. An explicit algorithm is favored for the central flow solver (CFS) because current codes have shown this class of solver to be appropriate for all current propelling charges except those in which tube wall boundary layers or very thin reaction layers are of interest. The FCT approach is favored because of its ability to resolve strong gradients without the introduction of numerical oscillations. Moreover, FCT can be made implicit if necessary in special cases. Finally, the choice of algorithm reflects current experience in respect to the exploitation of massively parallel computer architectures.

4.1 Balance Equations. Essentially, we view the flow as consisting of a multicomponent fluid, which may be either gas or liquid, and an aggregate of droplets or solid particles. In the earliest multiphase continuum models of solid propellant interior ballistics, it was customary to refer to the fluid as the "gas phase" and the aggregate as the "solid phase." As greater attention was given to the possibility of finite rate chemical processes, the term "gas phase" was replaced by the term "combustion products" and this was understood to admit the possibility that the decomposition of the propellant resulted in the local formation of incomplete combustion products which might be in the form of a gas, a vapor, or minute droplets or particles. This more general view is maintained here. However, we use the terms "continuous phase" and "discrete phase" to partition the flow. The continuous phase is understood to be a multi-component mixture of gases and liquids in local thermal equilibrium. The continuous phase is characterized by single local values of density, ρ; velocity vector, $\mathbf{u}$, temperature, T; pressure, p; shear stress tensor, τ; and internal energy, e. It is assumed to comprise N_c species, each characterized by local values of mass fraction Y_i and molar fraction X_i, $i = 1,\ldots,N_c$. Moreover, the velocity $\mathbf{u}$ is understood to be the barycentric or mass weighted average of the velocities of each of the components [48,49]. Each component is characterized by a diffusion velocity $\mathbf{v}_i$ relative to the barycentric value $\mathbf{u}$.

The term "discrete phase" is understood to refer to an aggregate of particles or droplets. If a solid propellant charge is being modeled, each type of propellant will constitute a component of the dispersed phase. Other components may be present if the decomposition of the propellant or an igniter element yields intermediate combustion products in particulate or droplet form. Still other components may need to be considered if rupture of a container is to be modeled or if wear-reducing additives like talc are present and their dispersal pattern is to be calculated. In the case of the RLPG, the aggregate may consist of a spray created by the breakup of the injected jet of liquid propellant. Similarly, in the ETCG or BLPG, the aggregate may consist of droplets created by the Helmholtz instability on the boundary of the Taylor cavity.

We assume that the discrete phase consists of a total of N_d components. Each component is characterized by density, ρ_{d_i}; stress tensor, σ_{d_i}; velocity vector, u_{d_i}; temperature, T_{d_i}; number density, n_{d_i}; and morphological data to characterize the volume, V_{d_i}, and surface area, S_{d_i} of each particle or droplet. The significance of the temperature T_{d_i} will depend on the model assumptions for component i. For very small droplets or particles, as might occur in a spray, T_{d_i} may be a bulk temperature. If component i corresponds to large particles for which the thermal penetration depth is small compared to the characteristic particle dimensions, then T_{d_i} may be a surface temperature. In such cases, it will be implicitly understood that T_{d_i} results from the analysis of the heat conduction equation applied to the exterior of the particle. In certain cases, it may also be necessary to consider the possibility of subsurface heat release due to condensed-phase reactions. We also note that the importance of internal circulation within spray droplets has been emphasized in certain cases [49]. This level of detail is not pursued in the present formulation. Similarly, in the discussion here we do not address the dual-voidage formulation of the flow through unslotted, perforated stick charges as has been presented elsewhere by Gough in the context of both one-dimensional [50] and two-dimensional models [14].

4.1.1 Microscopic Balance Equations. We consider now the formulation of the balance equations for the continuous and dispersed phases. On a sufficiently small scale of resolution in both space and time, we suppose that the continuous phase is represented by the balance equations for a multicomponent mixture as formulated by Williams [48], recast slightly to conservation or divergence form as in reference 29. Thus, we have the balances of mass, momentum, and energy in the forms

$$\frac{\partial \rho}{\partial t} + \nabla \cdot (\rho \mathbf{u}) = 0 \quad , \tag{1}$$

$$\frac{\partial}{\partial t}[\rho \mathbf{u}] + \nabla \cdot [\rho \mathbf{u}\mathbf{u} - \sigma] = 0 \quad , \tag{2}$$

$$\frac{\partial}{\partial t}\left[\rho(e + \frac{u^2}{2})\right] + \nabla \cdot \left[\rho \mathbf{u}(e + \frac{u^2}{2}) - \mathbf{u} \cdot \sigma + \mathbf{q}\right] = 0 \quad . \tag{3}$$

The mass balance of the i-th species is given in the form

$$\frac{\partial}{\partial t}\left[\rho Y_i\right] + \nabla \cdot \left[\rho Y_i(\mathbf{u} + \mathbf{v}_i)\right] = \dot{\omega}_i \quad , \tag{4}$$

where $\dot{\omega}_i$ is the rate of production of species i by chemical reactions. We have also introduced the stress tensor σ such that

$$\sigma = -p\mathbf{I} + \tau \tag{5}$$

where $\mathbf{I}$ is the unit tensor. The quantity e is understood to be the total internal energy and to include the heat of formation.

We note that equations 1–5 neglect external or body forces. Normally, the effects of gravity are negligible in interior ballistic processes. We also neglect the influence of electromagnetic forces even though some future ETCG designs might well involve the generation of electromagnetic fields within the combustion chamber. Similarly, the analysis presented here is not intended to apply to the component of the ETCG in which the plasma is formed. Provision may be made for the coupling to such a region via the boundary conditions. We also note that the sign convention for the stress tensor σ implies that a tensile stress is positive, as is made clear by equation 5. The heat flux $\mathbf{q}$ may be assumed to include radiative transport and thermal and mass diffusion.

Due to their generality, equations 1–4 may also be applied to the interior of each droplet or particle in each of the discrete phases. It is convenient for our purposes to think of N_c as formally tabulating not only all the chemical species in the continuous phase, but also those in the dispersed phases.

At the microscopic level, we require that equations 1–4 be solved subject to boundary conditions which we may state in a general form as

$$\left[\rho(\mathbf{u} - \mathbf{w})\cdot\mathbf{n}\right]_2^1 = 0 \tag{6}$$

$$\left[\left[\rho\mathbf{u}(\mathbf{u} - \mathbf{w}) - \sigma\right]\cdot\mathbf{n}\right]_2^1 = 0 \tag{7}$$

$$\left[\left[\rho\left(e + \frac{u^2}{2}\right)(\mathbf{u} - \mathbf{w}) + \mathbf{q} - \mathbf{u}\cdot\sigma\right]\cdot\mathbf{n}\right]_2^1 \tag{8}$$

$$\left[\rho Y_i(\mathbf{u} + \mathbf{v}_i - \mathbf{w})\cdot\mathbf{n}\right]_2^1 = \dot{\omega}_{s_i} \tag{9}$$

where $\mathbf{w}$ is the velocity of a boundary separating states 1 and 2, $\mathbf{n}$ is a normal vector, and we use the notation $[\psi]_2^1 = \psi_1 - \psi_2$. We also assume continuity of the tangential components of velocity and traction. In equation 9, we formally include a surface source term for production of species i. This makes it possible to embed into the boundary condition changes in chemical composition which occur very close to the boundary surface. The foregoing boundary conditions may be applied to the external boundaries of the flow as well as to the boundaries between the phases.

4.1.2 Formal Averaging of the Microflow Equations. The presence of the dispersed phases makes the system 1–4 computationally intractable. Consider, for example, a typical 155-mm granular propelling charge which contains about 10^3 grains. Each grain is typically a right circular cylinder with seven perforations aligned with its axis of symmetry. Flow structure would have to be resolved at a minimum length scale of 1 mm since this is the diameter of the perforations. Since the grains are randomly packed, the resolution would be necessary in three-dimensional detail. Therefore, the mesh spacing would be required to be no greater than 0.1 mm, and possibly quite a bit smaller. Even assuming a value of 0.1 mm implies that ~10^6 mesh points would be required to cover the cross section of the tube. Prior to motion of the projectile, the chamber length is typically 1 m so that a total of 10^{10} computational cells would be required. Current optimized Navier-Stokes solvers for nonreacting flows have been reported to require approximately 20 μs per cell per step on a Cray Y-MP [51,52]. Accordingly, each integration step would require approximately 10^5 CPU second, or roughly 30 hours. If the time step is subject to the Courant-Friedrichs-Lewy (CFL) stability condition [53], then the time step would have to be

approximately 10^{-7} s. Since the interior ballistic event occupies typically 10^{-2} s, a total of 10^5 steps would be required. An implicit solver might reduce the number of steps, but would require more computing time per step. Even if we accept 10^3 steps as a very optimistic estimate subject to the same CPU time per step, a complete simulation would require of the order of 10^8 s, or a little over 3 years.

In the next section, we shall comment on the performance gains possible with alternative architectures to that of the Cray. However, it will be our position that fully three-dimensional simulations of the microflow in a granular charge will remain infeasible for quite some time. Furthermore, even if such a calculation were to be made, it would be based upon a particular representation of the initial arrangement of the propellant grains. The details of the calculation would not have statistical significance and a number of calculations would be required to average out the influence of the initial condition in order that predictions of charge performance be relevant to the overall design. Similar considerations apply to the modeling of the RLPG and the ETCG in which the dispersed phase consists of an aggregate of propellant droplets.

It is, therefore, the case that a macroscopic perspective of the flow is necessary in which the balance equations 1–4 are modified to reflect average properties of the flow on a scale which is large compared with the characteristic lengthscales of the individual particles or droplets. Even without the presence of the dispersed phase, averaging is required in order to accommodate the presence of turbulence.

The derivation of macroscopic balance equations for multiphase flow by means of a formal averaging procedure has been described by numerous authors [54,55,56,57]. The formulation described by Gough [57] introduces a normalized weighting function g(x,t) such that

$$\int_{-\infty}^{+\infty} \int_{-\infty}^{+\infty} g(y,\tau)\,dy\,d\tau = 1 \quad . \tag{10}$$

Each phase is assumed to occupy a volume $V_i(t)$ which is bounded by surface $A_i(t)$. Then the volume fraction of each phase is defined as

$$\alpha_i(x,t) = \int_{-\infty}^{+\infty} \int_{V_i(\tau)} g(y - x, \tau - t)\,dy\,d\tau \quad . \tag{11}$$

Corresponding to each microscopic state variable ψ_i for phase i, we may define a macroscopic quantity $<\psi_i>$ according to

$$<\psi_i(x,t)> = \frac{1}{\alpha_i(x,t)} \int_{-\infty}^{+\infty} \int_{V_i(\tau)} \psi_i(y,\tau) g(y - x, \tau - t) dy d\tau \quad . \tag{12}$$

Whereas ψ_i is only defined on V_i, $<\psi_i>$ is defined everywhere. The macroscopic formulation requires that certain field variables be averaged over the surface A_i rather than the volume V_i. The surface averages arise naturally from the microscopic interfacial boundary conditions and define the manner in which the bulk averages are influenced by interfacial phenomena.

Analogously to (11) we introduce the surface area per unit volume of phase i in the form

$$S_i(x,t) = \int_{-\infty}^{+\infty} \int_{A_i(\tau)} g(y - x, \tau - t) dy d\tau \tag{13}$$

and the surface average of ψ_i is given by $<\psi_i>_s$ where

$$<\psi_i(x,t)>_s = \frac{1}{S_i(x,t)} \int_{-\infty}^{+\infty} \int_{A_i(\tau)} \psi_i(y,\tau) g(y - x, \tau - t) dy d\tau \quad . \tag{14}$$

Although the foregoing definitions of macroscopic quantities are sufficient for the complete development of the balance equations, a formal simplification can be obtained by the introduction of a density weighted average $<\psi>_\rho$ such that

$$<\psi_i>_\rho = <\rho_i \psi_i> / <\rho_i> \quad . \tag{15}$$

This form of averaging is commonly used in turbulence modeling [49]. It eliminates the formal presence of a number of correlation terms and simplifies the others. The correlation terms take the form $<\psi'\phi'>$ where ψ' is the fluctuation about the average.

$$\psi' = \psi - \langle\psi\rangle \quad , \tag{16}$$

and similarly for ϕ'. Higher order correlations can also arise in the form $\langle\psi'\phi'\eta'\rangle$. Fluctuations can also be defined with respect to the density weighted average. By analogy to (16), we have

$$\psi^* = \psi - \langle\psi\rangle_\rho \quad . \tag{17}$$

We note the generality of the foregoing definition of the macroscopic variables. The weighting function is never specified explicitly. We simply require that it have as many continuous partial derivatives as we may need and that it tend to zero sufficiently rapidly as its arguments become infinite. Accordingly, the average may be thought of as a volume average, a time average, or a combination of the two. Furthermore, if the weighting function is sufficiently localized, we simply recapture the local values of the microproperties. The macroscopic equations are deduced by averaging the microflow equations and exploiting the rules of commutation between the averaging operator (12) and the differential operators. This procedure has been discussed in detail for various systems of microflow equations by several authors [54–57]. The derivation of the present system equations is discussed in detail by Gough [58]. Here we simply summarize the results.

4.1.3 Macroscopic Balance Equations. We use α to denote the porosity, or the fraction of a unit macroscopic volume occupied by the continuous phase. Similarly, we use α_{d_i} to denote the volume fraction of the i-th discrete phase. Evidently,

$$\alpha = 1 - \sum_{i=1}^{N_d} \alpha_{d_i} \quad . \tag{18}$$

Moreover, if the i-th discrete phase consists of n_{d_i} particles or droplets per unit volume and the volume of each particle is V_{d_i}, then we have

$$\alpha_{d_i} = n_{d_i} V_{d_i} \quad . \tag{19}$$

Similarly, the surface area per unit volume, equation 13, may be written as

$$S_i = n_{d_i} S_{d_i} \quad . \tag{20}$$

We note that n_{d_i}, like α_{d_i}, is a macroscopic or average quantity. The representation of equations 19 and 20 is appropriate when accurate knowledge of V_{d_i} and S_{d_i} is expected, as is usually the case with solid propellant charges.

We consider first the macroscopic equations for the continuous phase. We have the balance of mass in the form

$$\frac{\partial}{\partial t}[\alpha<\rho>] + \nabla \cdot \left[\alpha\rho<u>_\rho\right] = \sum_{i=1}^{N_d} \dot{m}_{d_i} \quad . \tag{21}$$

Here $\dot{m}_{d_i}$ is the rate of decomposition per unit volume of the i-th dispersed phase. If the dispersed phase consists of well-formed particles whose rate of surface regression is $\dot{r}_{d_i}$, then evidently

$$\dot{m}_{d_i} = n_{d_i} S_{d_i} <\rho_{d_i}><\dot{r}_{d_i}>_s \quad . \tag{22}$$

We note that equation 21 does not explicitly include a source term to represent an external ignition stimulus as has often been considered in previous models of solid propellant charges [11,14]. Such a term can be considered to be represented implicitly by one of the $\dot{m}_{d_i}$ with appropriate assumptions concerning its state of motion [58].

Each of the j components of the continuous phase satisfies a balance of mass equation in the following form,

$$\frac{\partial}{\partial t}\left[\alpha<\rho><Y_j>_\rho\right] + \nabla \cdot \left[\alpha<\rho><Y_j>_\rho(<u>_\rho + <v_j>_\rho)\right] + \nabla \cdot \left[\alpha<\rho><Y_j^{\bullet}(u^{\bullet} + v_j^{\bullet})>_\rho\right]$$

$$= \alpha<\dot{\omega}_j> + \sum_{i=1}^{N_d} \dot{m}_{d_i} <Y_{d_{ij}}>_s \quad . \tag{23}$$

Here $\langle Y_{d_{ij}} \rangle_s$ is the average mass fraction of species j produced by the decomposition of the i-th discrete phase including the effect of the surface reaction. In general, the definition of $\langle Y_{d_{ij}} \rangle_s$ will involve some prior judgment on the part of the modeler as to the rate of the gas-phase kinetics. Reactions which proceed faster than the local mixing process can be embedded into $\langle Y_{d_{ij}} \rangle_s$. It is often satisfactory to assume that thermochemical equilibrium is achieved at a distance from the surface which is small compared with the scale of heterogeneity, in which case the $\langle Y_{d_{ij}} \rangle_s$ may be specified in accordance with the equilibrium properties of the products of decomposition.

We also note, in equation 23, the appearance of a correlation term on the left-hand side. The formal average includes as a special case a local time average of the type used to derive the governing equations for single-phase turbulent flow. Accordingly, we may identify the correlation terms which appear in the present system of equations with their counterparts in the theory of turbulence. The correlation term in equation 23 may therefore be interpreted as the turbulent transport of species j with respect to the mean continuous phase velocity $\langle \mathbf{u} \rangle_\rho$.

The macroscopic balance of momentum for the continuous phase takes the form,

$$\frac{\partial}{\partial t}\left[\alpha\langle\rho\rangle\langle\mathbf{u}\rangle_\rho\right] + \nabla\cdot\left[\alpha\langle\rho\rangle\langle\mathbf{u}\rangle_\rho\langle\mathbf{u}\rangle_\rho\right]$$

$$= -\alpha\nabla\langle p\rangle + \alpha\nabla\cdot\langle\tau\rangle - \nabla\cdot\left[\alpha\langle\rho\rangle\langle\mathbf{u}^{\bullet}\mathbf{u}^{\bullet}\rangle_\rho\right] + \sum_{i=1}^{N_d}\dot{m}_{d_i}\langle u_{d_i}\rangle - \sum_{i=1}^{N_d} n_{d_i} S_{d_i} \mathbf{f}_{d_i} \quad . \tag{24}$$

Here $\mathbf{f}_{d_i}$ represents the force per unit surface area on the i-th discrete phase due to motion relative to the continuous phase. The formal definition of $\mathbf{f}_{d_i}$ is given by

$$n_{d_i} S_{d_i} \mathbf{f}_{d_i} = -\int_{-\infty}^{\infty}\int_{A_i(\tau)} g\sigma'\cdot\mathbf{n}\,da\,d\tau \tag{25}$$

where A_i is the surface of the i-th discrete phase, σ' is the fluctuation of the continuous-phase stress tensor and $\mathbf{n}$ is the unit outward facing normal for the i-th discrete phase. We will interpret this term as the interphase drag and discuss appropriate constitutive laws to relate it to the macroscopic state variables.

We note that equation 24 differs from that used by other authors [18,56] in respect to the divergence of the stress deviator. Other authors have $\nabla \cdot \alpha \langle \tau \rangle$ where we have $\alpha \nabla \cdot \langle \tau \rangle$. This point is discussed further in reference 58. The form used here is consistent with the formal definition (25). It is not likely that the differences in the representation of the macroscopic stress divergence will have material modeling consequences when the present level of uncertainty concerning the constitutive laws is taken into account. We also note on the right-hand side of equation 24 the presence of the correlation term $\nabla \cdot \alpha \langle \rho \rangle \langle \mathbf{u}^{\bullet} \mathbf{u}^{\bullet} \rangle_{\rho}$. By analogy to the theory of turbulence, we may interpret this as a Reynolds stress which expresses the transfer of momentum by the fluctuation field.

The energy equation for the continuous phase takes the form

$$\frac{\partial}{\partial t}\left\{\alpha\langle\rho\rangle\left[\langle e\rangle_{\rho} + \frac{1}{2}\langle u\rangle_{\rho}^{2}\right]\right\} + \nabla\cdot\left\{\alpha\langle\rho\rangle\langle u\rangle_{\rho}\left[\langle e\rangle_{\rho} + \frac{1}{2}\langle u\rangle_{\rho}^{2}\right]\right\}$$

$$= \nabla\cdot\alpha\langle u\rangle_{\rho}\cdot\langle\sigma\rangle - \nabla\cdot\alpha\langle q\rangle - \langle p\rangle\frac{\partial\alpha}{\partial t}$$

$$- \sum_{i=1}^{N_d} n_{d_i} S_{d_i} \langle q_{d_i}\rangle_s - \sum_{i=1}^{N_d} n_{d_i} S_{d_i} \mathbf{f}_{d_i}\cdot\langle \mathbf{u}_{d_i}\rangle_{\rho}$$

$$+ \sum_{i=1}^{N_d} \dot{m}_{d_i}\left(\langle e_{d_i}\rangle + \frac{\langle p\rangle}{\langle\rho_{d_i}\rangle} + \frac{\langle u_{d_i}\rangle^2}{2}\right) - \Theta \quad , \tag{26}$$

where the correlation term Θ is given by

$$\Theta = \nabla\cdot\alpha\langle \mathbf{u}^{\bullet}\cdot\sigma\rangle + \frac{\partial}{\partial t}\left\{\alpha\langle\rho\rangle\frac{\langle \mathbf{u}^{\bullet}\cdot\mathbf{u}^{\bullet}\rangle_{\rho}}{2}\right\}$$

$$+ \nabla\cdot\left\{\alpha\langle\rho\rangle\left[\langle \mathbf{u}^{\bullet} e^{\bullet}\rangle_{\rho} + \langle u\rangle_{\rho}\frac{\langle \mathbf{u}^{\bullet}\cdot\mathbf{u}\rangle_{\rho}}{2} + \langle u\rangle_{\rho}\cdot\langle \mathbf{u}^{\bullet}\cdot\mathbf{u}^{\bullet}\rangle_{\rho}\right.\right.$$

$$\left.\left. + \langle \mathbf{u}^{\bullet}\frac{\mathbf{u}^{\bullet}\cdot\mathbf{u}^{\bullet}}{2}\rangle_{\rho}\right]\right\} \quad . \tag{27}$$

We note the phase interaction terms on the right-hand side of equation 26. The first of these introduces the heat transfer due to conduction and radiation per unit surface area $<q_{d_i}>_s$. The next term represents the work done by the interphase drag. The third term represents the heat added due to decomposition of the discrete phases. The correlation term Θ is seen to be very complicated. In general, most of the terms in Θ will be neglected with the exception of the dissipation term contained in $\nabla \cdot \alpha <\mathbf{u}^* \cdot \sigma>$, which may be interpreted as yielding a rate of dissipation of turbulent kinetic energy [18], and the diffusion term $\nabla \cdot \left[\alpha <\rho><\mathbf{u}^* e^*>_\rho \right]$.

The i-th dispersed phase is found to be governed by a macroscopic mass balance analogous to that for the continuous phase, namely,

$$\frac{\partial}{\partial t}\left[\alpha_i <\rho_{d_i}> \right] + \nabla \cdot \left[\alpha_i <\rho_{d_i}><\mathbf{u}_{d_i}>_\rho \right] = - \dot{m}_{d_i} \quad . \tag{28}$$

We note that no provision is made in equation 28 for the transformation of one discrete phase into another. Such processes may occur if the discrete phases constitute a spray in which droplets may combine or be shattered [59]. Current interior ballistic models do not reflect these complexities due to a lack of reliable characterization of droplet size distributions in the sprays which can occur in the designs based on liquid propellants. The balance equations may be easily amended if such processes prove to be of concern at some future time.

The i-th dispersed phase is governed by a macroscopic balance equation in the following form

$$\frac{\partial}{\partial t}\left[\alpha_i <\rho_{d_i}><\mathbf{u}_{d_i}>_\rho \right] + \nabla \cdot \left[\alpha_i <\rho_{d_i}><\mathbf{u}_{d_i}><\mathbf{u}_{d_i}> \right]$$

$$= - \alpha_i \nabla <p> + \nabla \cdot \left[(1 - \alpha)\left(<p>\mathbf{I} + <\sigma_{d_i}> \right) \right] + n_{d_i} S_{d_i} \mathbf{f}_{d_i} - \dot{m}_{d_i} <\mathbf{u}_{d_i}>_\rho \quad . \tag{29}$$

We note on the right-hand side of equation 29, the formal presence of a stress term $<p>\mathbf{I} + <\sigma_{d_i}>$ which reflects the difference between the average stress in the i-th dispersed phase and the average ambient pressure in the continuous phase. This is interpreted as reflecting interactions between droplets or particles. No correlation term analogous to that in the continuous phase momentum equation is considered here. Fluctuations in velocity about the mean are neglected for the dispersed phases. This does not

however preclude the consideration of turbulent transport of the i-th dispersed phase as a consequence of the turbulence in the continuous phase. Such a coupling would be reflected in the constitutive law for $\mathbf{f}_{d_i}$ as we discuss further, subsequently.

The dispersed phases do not require an energy balance analogous to that for the continuous phase. The dispersed phases consist of condensed media in which the temperature is essentially uncoupled from the macroscopic dilatation. An analysis of the temperature of the dispersed phases is required on a microscopic basis with the heat transfer from the continuous phase acting as a boundary condition for the heat conduction equation applied to the interior of each droplet or particle. We view this topic as an aspect of the constitutive laws which are used to model the interphase heat and mass transfer.

As we discuss further in the context of the constitutive laws, equation 29 may not necessarily be solved directly for each of the dispersed phases. If the i-th dispersed phase is defined as being in mechanical equilibrium with the continuous phase—as may be the case if the particles or droplets are very small—then the momentum equation for the i-th phase may be simply added to that for the continuous phase thereby eliminating $\mathbf{f}_{d_i}$ as an unknown. In such a case, moreover, it would be assumed that $-<\sigma_{d_i}> = -<p>\mathbf{I}$. Even the continuity equation 28 may be replaced by an alternative formulation in the context of obtaining numerical solutions. As we shall discuss subsequently, there are distinct numerical advantages to replacing equation 28 by a direct average of the dispersed phase distribution in order to deduce the volume fraction α_{d_i}.

It is thought that the foregoing system of balance equations includes all the systems presently used to model the various types of propelling charges of current interest. Differences between the various systems are confined to the constitutive laws, the boundary conditions, and the complexity of the geometrical domain in which the solution is to be obtained. We now proceed to a discussion of these topics referring in each case to the choices appropriate to each of the major types of propelling charge.

4.2 Constitutive Laws. The macroscopic balance equations require a number of constitutive laws for closure. These include laws governing the molecular and turbulent transport terms; the equation of state of the continuous phase; the rates at which chemical reactions proceed; the law governing the intergranular stresses; equations to describe the morphology of the dispersed phases; and finally, the laws governing the interphase transfers of momentum, energy and mass. We discuss each of these topics in the foregoing

order. It should be kept in mind that an express goal of the next-generation code is to admit revisions to the constitutive laws when occasion demands. Accordingly, the results given here are not intended to be either exhaustive or exclusive. They are intended to reflect current modeling practices in each of the areas of current interest. Further details are given in reference 58.

4.2.1 Molecular Transport Terms. Generally speaking, these terms are not considered in current models of solid propellant gun (SPG) interior ballistics unless attention is given to the tube wall boundary layer. They may be of interest in simulations of the RLPG when attention is given to the behavior of oscillations in the combustion chamber, although their turbulent counterparts would be expected to dominate. Transport is of concern in the ETCG and BLPG, but turbulence is again expected to exert a dominant effect. The molecular transport processes are reflected in three terms, namely, the shear stress term τ; the heat flux vector $\mathbf{q}$; and the diffusion velocities $\mathbf{v}_i$. We first consider the laws which pertain at the microscale, or, alternatively, in the absence of the dispersed phases.

We take the shear stress tensor to obey the Navier-Stokes relation [48,49],

$$\tau = \mu\left(\nabla \cdot \mathbf{u} + \nabla \cdot \mathbf{u}^{\mathsf{T}}\right) + \left(\mu' - \frac{2}{3}\mu\right)\mathbf{I}\nabla \cdot \mathbf{u} \quad , \tag{30}$$

where μ is the molecular viscosity and μ', the bulk viscosity, is normally neglected unless strong departures from the thermodynamic equilibration occur. We use $\nabla \cdot \mathbf{u}^{\mathsf{T}}$ to denote the transpose of $\nabla \cdot \mathbf{u}$. The heat flux vector may be written as [29,49]

$$\mathbf{q} = -\lambda \nabla T + \rho \sum_{i=1}^{N_c} h_i Y_i \mathbf{v}_i + \mathbf{q}_{rad} \quad , \tag{31}$$

where λ is the thermal conductivity, $h_i = e + p/\rho$ is the enthalpy, T is the temperature, and $\mathbf{q}_{rad}$ is the radiative component. The Dufour heat flux has been omitted from equation 31 on the assumption that it will be negligible. Radiative heat transfer, which may be of importance in the ETCG, may be resolved according to the diffusion approximation on the assumption that the gas in the gun chamber will be optically thick. We have [29,60]

$$\mathbf{q}_{rad} = -\frac{4\sigma}{3\alpha_R} \nabla T^4 \quad , \tag{32}$$

where σ is the Stephan-Boltzman constant and α_R is referred to as the Rosseland mean absorption coefficient. The diffusion velocity, v_i, is assumed to obey Fick's Law in the form [49]

$$v_i = - D\rho \nabla Y_i \quad . \tag{33}$$

Equations 30–33 express the molecular transfer laws in the absence of the dispersed phases. They may be transformed to macroscopic relations by means of the formal averaging technique discussed in the previous section. Results for a single component fluid are presented by Ishii [56] and by Gibeling and MacDonald [18]. The extension to a multicomponent fluid is discussed by Gough [58].

4.2.2 Turbulent Transfer Terms. The comments in the preceding discussion of the relevance of the molecular transport terms in the modeling of various propelling charge configurations apply equally well to the turbulent terms. As with the molecular terms, it is natural to look first to the situation in which the dispersed phases are not present in order to define appropriate constitutive laws. The general approach is to formulate a law for the turbulent transport of momentum by analogy to that for the molecular process, thereby introducing a turbulent viscosity. The corresponding transport coefficients for energy and mass follow from laws of similitude. The simplest models for the turbulent viscosity are based on algebraic laws [61] and no consideration is given to the dissipation of turbulent kinetic energy in the mean flow energy balance. Although such laws are relatively simple to use, they are inappropriate to the dynamic situation which occurs in a gun except in special cases. Accordingly, interest is focussed on a two-parameter turbulence law [18,39,62], reflecting the assumption that the dissipation of turbulent kinetic energy occurs at the Kolmogarov microscale [63]. We take the Reynolds stress to be related to the mean flow properties and the turbulent kinetic energy by the relation

$$<\rho><u''u''>_\rho = \frac{2}{3}(\mu_T \nabla \cdot <u>_\rho + <\rho>k) - \mu_T(\nabla \cdot <u> + \nabla \cdot <u>^T) \quad , \tag{34}$$

where $k = \frac{1}{2}<u''u''>_\rho$ is the turbulent kinetic energy and μ_T is the turbulent viscosity. The turbulent bulk viscosity has been neglected in equation 34. The turbulent viscosity is given by

$$\mu_T = C_\mu <\rho> k^2/\epsilon \tag{35}$$

where C_μ is an empirical constant and ϵ is the rate of dissipation of turbulent kinetic energy

$$\epsilon = \frac{<\tau : \nabla u''>}{<\rho>} \tag{36}$$

In general, k and ε are determined by time-dependent partial differential equations [39,62]. We note, however, that Gibeling and McDonald suggested the use of an algebraic law for the dissipation rate in conjunction with a specified turbulence lengthscale [18]. Once μ_T is known, the remaining turbulent diffusion terms are resolved according to

$$<\rho><u''\psi''>_\rho = -\frac{\mu_T}{\sigma_T}\nabla<\psi> \quad , \tag{37}$$

where ψ is an arbitrary scalar and σ_T is a dimensionless coefficient which is normally referred to as the Prandtl number if ψ represents energy and the Schmidt number if ψ represents mass.

The relations 34–37 are intended to describe the structure of turbulence in the absence of the discrete phases. As with the molecular laws, formal averaging can be applied to account for the presence of the particles. However, it is not clear that the production of turbulence by the dispersed phases will be captured properly by this formal process [58].

4.2.3 Equation of State of Continuous Phase. We require relations to describe the thermal equation of state

$$p = p(\rho, T, Y_i) \quad , \tag{38}$$

and the caloric equation of state which we write in the form

$$e = e(\rho, T, Y_i) \quad . \tag{39}$$

It is understood in equations 38 and 39 that Y_i stands for $Y_1, Y_2, \ldots, Y_{N_c}$. In much of the modeling work that has been done on SPG and RLPG charges, the continuous phase has been assumed to consist of a gas and the covolume law has been used in the simple form

$$p = \frac{\rho R T}{(1 - b\rho)} \tag{40}$$

$$e = c_v T \tag{41}$$

where R is the gas constant defined by $R = R_u/M_w$, where R_u is the universal gas constant and M_w is the molecular weight of the gas; c_v is the specific heat at constant volume; and b is the covolume. Appropriate constant values have been used based on a fitting to the equilibrium properties of the products

of composition of the propellant determined by the BLAKE Code [64]. Equations 40 and 41 exhibit no dependence on composition. When composition dependence is required one may extend 40 and 41 by setting the covolume, the specific heats and the reciprocal of the molecular weight equal to mass weighted averages of the properties of the constituent species and by replacing 41 with the relation

$$e = \sum_{i=1}^{N_c} \left\{ h_{i_o} + \int_{T_o}^{T} c_{p_i}(T)dT \right\} + b(p - p_o) - \frac{p}{\rho} \quad . \tag{42}$$

where h_{i_o} is the heat of formation of species i at constant pressure and reference temperature T_o and pressure p_o, and c_{p_i} is the specific heat at constant pressure of the i-th constituent.

The most complex considerations arise in the context of the ETCG. These charges may involve continuous species in virtually any material state, condensed, gas, or plasma. An approach to combining the properties of the constituents to obtain the overall properties of the continuous phase in an ETCG has been recently described by Su and Stock [65].

Current practice is to assume that the microflow equation of state applies equally well on the macroscale so that correlations which arise from the formal averaging of the relations 40–42 may be neglected.

4.2.4 Reaction Rates in the Continuous Phase. The chemical reaction rates may be assumed to follow standard Arrhenius relations [29] which do not need to be repeated here. In some cases where a discrete phase is assumed to be in mechanical equilibrium with the continuous phase, an overall mixture formulation may be used in which case the reaction rate may be specified in a pressure dependent form to reflect droplet or particle burning.

4.2.5 Equation of State of Discrete Phases. We note that the momentum equation for the discrete phases contains a term which we denote by

$$\langle \sigma_{s_i} \rangle = -\langle p \rangle \mathbf{I} \cdot \langle \sigma_{d_i} \rangle \quad . \tag{43}$$

The simplest assumption that one may make concerning $\langle \sigma_{s_i} \rangle$ is that it vanishes. This will be reasonable if the discrete phase consists of dispersed droplets or particles and the Mach number of the continuous

phase is small compared with unity. In such a case, we expect the average stress in the particles to equal the ambient pressure in the continuous phase. This assumption is pertinent in the cases of the RLPG and the ETCG. However, when the particles are in contact with one another, as is the case initially in SPG charges, we assume that $<\sigma_{s_i}>$ is not zero and, in fact, embeds the intergranular stresses.

We refer to the discussion by Gough who formulated an isotropic rheological relation in the form

$$<\sigma_{s_i}> = <\sigma_{s_i}>(\alpha_i, \dot{\alpha}_i) \tag{44}$$

for beds of granular propellant [11]. For two-dimensional modeling of stick propellant, an anisotropic law was formulated [14]. Both these laws may be thought of as equilibrium relations. In the related area of deflagration-to-detonation transition (DDT) in porous propellants, non-equilibrium relations may be required due to the high rates of deformation. The work of Kooker [66] may be consulted in this regard.

4.2.6 Morphology of Discrete Phases. Closure of the balance equations requires knowledge of the surface area per unit volume of the dispersed phases. In all work to date it has been assumed that knowledge of the volume and surface area of individual particles or droplets was available. This is a safe assumption in the context of the SPG since the grains are formed with some precision in order to assure control of the ballistic process. In these charges the required relations follow from straightforward geometrical considerations given the initial grain geometry and the surface regression at each time, the latter being assumed uniform over the surface of each grain.

For the RLPG and the ETCG, the situation is not so well defined. Indeed, conditions in the chamber may become supercritical at which point it can no longer be safely assumed that the spray consists of spherical droplets, as the surface tension disappears. It is likely that droplets of various sizes exist and consideration of a local droplet size distribution is necessary in principle. We note that the present formulation supports such a contingency since the size distribution may be discretized in such a way as to associate the aggregate with a number of discrete phases. Transitions between the discrete phases would then have to be included. At present, the poor state of knowledge of the spray properties has confined the characterization of the surface area per unit volume to an average of the local aggregate. A review of relations to characterize mean droplet size in the RLPG has been presented by Coffee et al. [67].

4.2.7 Interphase Momentum Transfer. The momentum equation for the discrete phases contains two gas dynamic forces on the right-hand side. The first involves the macroscopic pressure gradient and may be interpreted as a buoyancy effect. The second term involves $\mathbf{f}_{d_i}$, a surface integral of the normal component of the stress fluctuation tensor, and which is interpreted as embedding the effect of relative motion of the phases. In almost all modeling work to date, it has been assumed that $\mathbf{f}_{d_i}$ is a function of the local Reynolds number based on a characteristic particle length, the volume fraction α and the relative velocity $\mathbf{u} - \mathbf{u}_{d_i}$. The functional dependence is determined by fitting to experimental data based on steady flow. Specific formulations appropriate to stick and granular charges may be found in the report by Gough [11]. For multidimensional modeling of stick propellant, it is necessary to formulate an anisotropic law of flow resistance [14]. For the RLPG and ETCG in which the discrete phases are droplets, the various authors have used a variety of laws.

In early work, it was thought appropriate to include in $\mathbf{f}_{d_i}$ the effect of virtual mass [55]. However, subsequent efforts have neglected this term due to lack of knowledge of appropriate coefficients for a packed bed of propellant. For small, dispersed particles or droplets, the virtual mass effect should be considered. In a study of turbulent transfer of minute particulates in a gun, Buckingham included not only virtual mass but also the Basset and Saffman forces [68]. For small particles, moreover, coupling to the turbulent component of velocity may be of importance. This is true not only in the problem of dispersal of wear-reducing additives [68] but also in the ETCG. Chen [39] describes the application of the formulation of Dukowicz [69] to the modeling of the spray in an ETCG design.

4.2.8 Interphase Heat and Mass Transfer. During the early stages of flamespreading in an SPG, the dominant process is heat transfer to the solid propellant due to convection and, to a lesser extent, radiation. During the early stages, the propellant is not burning and mass transfer does not occur. The convective heat transfer is resolved from empirical correlations which are predicated on the mean flow properties. The radiative component follows from the usual dependence on $\langle T \rangle^4 - \langle T_{d_i} \rangle_s^4$ where $\langle T_{d_i} \rangle_s$ is the surface temperature of the i-th discrete phase. Representative formulae may be found in the work of Gough [11,14]. The surface temperature is found from a solution of the one-dimensional heat conduction equation applied to the interior of the propellant with the interphase heat flux as a boundary condition. In the simplest models of SPG ignition and combustion, it is assumed that ignition occurs when the surface temperature reaches a predetermined value. Subsequently, the surface is assumed to regress at a rate determined by the ambient pressure in accordance with empirical data. No model of the combustion

process is involved. The propellant is assumed to decompose to final equilibrium products close to the surface. These conditions then determine the interphase heat and mass transfer following ignition.

A similar approach may be used to describe the combustion of monopropellant sprays in the RLPG and ETCG. For designs which involve bipropellants, a somewhat different model is required. For example, if the spray consists of fuel droplets, an evaporation rate may be determined from the heat transfer rate. The evaporating fuel may then react with the oxidizing ambient in the macroscale. Attention may also be required to a near-field effect which will modify the overall rate of heat transfer with respect to the values obtained for inert droplets. The work of Chen may be consulted for a discussion of such a model [70].

Similarly, more complex models of heat and mass transfer can be formulated for the SPG. The rate of regression of the surfaces may be determined from a pyrolysis or an evaporative law in combination with a near-field flame model and a time-dependent solution of the heat conduction equation applied to the interior of the grain. The near-field products of decomposition need not be at equilibrium and may react on the macroscale [71].

4.3 Boundary Conditions. We partition the boundary conditions into two categories, external and internal. The external boundary conditions apply at surfaces beyond which the numerical solution is not pursued. Ordinarily in the simulation of the interior ballistics of the SPG, these surfaces include the breechface, the tube wall, and the base of the projectile. Usually the boundary conditions consist of statements of tangential slip of both phases and no normal penetration. However, if a reactive sidewall is present, then flux boundary conditions may be specified. Flux boundary conditions may also apply at the surface of an igniter tube which may extend into the chamber. Ordinarily, the projectile is treated as a rigid body which may rotate about its axis and its surfaces are treated as impermeable. It is possible that fins might be present and that modeling of ablation of the fins would be required, thereby leading to a flux boundary condition. A flux boundary condition would also apply at the base of the projectile if it were an inbore rocket.

The foregoing discussion applies when interest is focussed on the ballistics of the charge. If interest is focussed on the tube wall boundary layer, then no slip conditions apply to the continuum phase on those surfaces which are inert. The heat flux has to be coupled to the thermal response of the tube.

If we limit our domain of integration to the combustion chamber and tube of the gun, the preceding remarks apply equally well to the RLPG and the ETCG. However, we need to consider a flux boundary condition on those parts of the surface at which injection of propellant or plasma occurs. These injection ports may be located arbitrarily.

The internal boundaries refer to surfaces within the overall computational domain at which two distinct regions are coupled. In modeling the SPG, Gough [11,14] has treated the charge increment boundaries as macroscopic discontinuities across which jumps occur in all the state variables. The flows on each side of the boundary are coupled via explicit jump conditions. Moreover, in modeling artillery charges for which the increments are loaded in bags or other containers, the properties of the containers have been embedded into the jump conditions.

An internal boundary condition will arise in the RLPG if the boundaries of the injected jets of propellant are modeled explicitly. To the author's knowledge this has not been done. An internal boundary may be defined in the ETCG if the Taylor cavity is modeled explicitly. Such a model has been formulated by Chen [70], but solutions have been confined to a simpler representation. Other authors have not resolved the cavity boundary explicitly.

Further discussion of the boundary conditions with special reference to the SPG is contained in reference 58.

4.4 Method of Solution. The system of equations described in the previous section is clearly of the most general type and admits a full range of fluid-dynamic behavior. It is unfortunately the case that there is no single best way to solve such equations. Depending on the nature of the solution itself, certain categories of solution technique will offer particular advantages in terms of accuracy or computer resources, advantages which may accrue to a different category if the structure of the flow is altered. Because the advantages of particular methods of integration are problem dependent, it is our view that the next generation code should admit the possibility of multiple flow solvers, each having application to particular areas of concern. At the same time, it is clearly desirable that the number of solvers be kept to a minimum, for the sake of simplicity and to promote portability. In particular, we believe that it is of great importance that a central flow solver be established which combines simplicity of structure with a maximum scope of applicability. It is not desirable to complicate the structure of the central flow solver with features which are required only in specialized circumstances. Separate solvers can be developed for

special cases without the same constraints of maximum portability from computer system to computer system and from user to user.

The present discussion focusses on the structure of a CFS for the next-generation code. We first review some general factors which determine broad criteria for the selection of a central algorithm. We then define the structure of the next-generation code, considering not only the CFS but also the additional modules which may be foreseen as necessary to treat particular situations which are outside the scope of the central flow solver.

4.4.1 General Considerations. Since the balance equations constitute a system of partial differential equations, it is taken for granted that solutions will be determined using some sort of finite difference representation. Accordingly, we suppose that the physical domain, on which the solution is to be determined, is to be covered by a mesh and that values of the state variables will be determined either at the mesh points which define the vertices of each computational cell or at the center of each such cell. We distinguish between structured and unstructured meshes. We may define a two-dimensional mesh as structured if the physical domain can be mapped onto a unit square in such a way that the mesh points transform into a regularly spaced array in both directions. In three dimensions, we consider mapping onto a unit cube. We refer to the unit square or unit cube as the "computational domain." A variety of techniques are available to map irregular physical domains onto regular computational domains. In some cases, the physical domain may be partitioned into a number of subregions each of which is then transformed onto a regular computational domain. The advantage of a structured mesh is associated with the simplicity with which the data used to represent the solution are stored in the memory of the computer. The data required to form finite difference representations of the spatial derivatives for a given cell are all available locally and are related to the cell coordinates by simple fixed rules which do not vary from cell to cell. Unstructured meshes do not admit simple rules to relate the vertices of each cell to the cell coordinates. Instead, each cell is characterized by a list of mesh points which constitute its corners, the number of points depending on the geometry of the cell which is usually either triangular or quadrilateral. The advantage of the unstructured mesh is its adaptability to very complex physical domains and the ease with which local mesh refinement can be incorporated whenever the structure of the solution so demands.

A second broad distinction between numerical methods relates to the determination of the spatial derivatives. If the derivatives are represented in terms of current data, the scheme is said to be explicit. The significance of the explicit representation is that the updated values of the state variables depend only

on current values at the mesh point in question and certain of its nearest neighbors. However, explicit schemes are subject to stability criteria which constrain the time step. Ordinarily, the most stringent criterion is the Courant-Lewy-Friedrichs (C-F-L) condition which requires the timestep to be less than a characteristic cell dimension divided by the fastest wavespeed [53]. A scheme is said to be implicit when the spatial derivatives are determined entirely or in part by the future values of the state variables. Implicit schemes can be made unconditionally stable. However, the future values are all coupled and a matrix inversion is required to complete the solution. In addition, implicit schemes incorporate an unphysical linkage of future values which may violate principles of causality. The question of whether to use an explicit or an implicit scheme turns principally on the structure of the flow. For problems in which wave propagation is of primary concern, the flow may be well resolved with a mesh whose physical spacing is more or less uniform. Resolution of the time dependence demands that the timestep be given a value comparable to that required by the C-F-L stability condition. In such a case, the C-F-L stability constraint is not a limiting factor and the additional cost and complexity of an implicit scheme is not justified. On the other hand, if the flow contains structure on a very fine lengthscale, as for example when the tube wall boundary layer is to be determined, the C-F-L stability criterion can be unduly restrictive and an implicit solution technique may not only be justified but may in fact represent the only feasible means of obtaining a solution. For example, the results presented by Garloff and Heiser [61] were based on a timestep which exceeded the C-F-L limit by a factor of 5,000.

The foregoing distinction between explicit and implicit representations has focussed exclusively in the spatial derivatives. The balance equations also contain source terms which reflect the rate of chemical reactions or the interphase coupling processes. These too may be represented either explicitly or implicitly for reasons of stability. Since they involve only local variables, there is no linkage to other mesh points and implicit treatment of these terms does not lead to a requirement that a matrix be inverted.

A third distinction between methods of solution relates to the manner in which internal discontinuities are treated. For single phase flows, it is customary to view shock waves and contact surfaces as discontinuities since their structure is confined to a layer whose thickness is of the order of the mean free path and, therefore, at the limit of the resolving power of the continuum equations. In multiphase flows, which are described by macroscopic equations, one may also view the boundary of a granular aggregate as a surface of discontinuity since the volume fraction will change by a finite amount over a layer whose thickness is comparable to the scale of heterogeneity, the lengthscale which defines the resolving power of the averaged equations. We distinguish between methods of solution which capture discontinuities and

those which represent them explicitly. Methods which represent the discontinuities explicitly track the surfaces as internal boundaries and apply the finite jump conditions to match the boundary values on each side. Methods which capture the discontinuities do so by representing them as regions of strong gradients so that the surface is spread out over several cells. The capturing technique has the advantage of being simple to encode and the disadvantage of being less accurate. Larger numbers of cells may be required in a capturing technique in order to effect adequate localization of the smeared surfaces.

The foregoing discussion has addressed broad differences in the various techniques of solution without reference to the architecture of the computer on which the solution technique is to be implemented. Until recently, computers consisted of one powerful processor which was required to act locally on a stream of instructions applied to data distributed throughout memory. At the present time, a variety of architectures are available [52]. Figure 6 illustrates the characteristics of some of the presently available and planned computers. The figure includes several massively parallel architectures in which a large number of processors are available to work concurrently. These may be distinguished as either multiple-instruction, multiple data (MIMD) or single-instruction, multiple data (SIMD) architectures. MIMD computers allow each processor to perform different instructions on different data. SIMD computers have each processor perform the same series of instructions but on different data. The SIMD architecture is best suited to formulations of fluid dynamics problems which depend on nearest neighbor interactions since a time penalty is paid for accessing remote data.

We have noted that the lumped parameter codes which originated some 30 years ago are still used on a frequent basis today. The one-dimensional XKTC Code is nearly 20 years old and continues to be developed and applied. Whereas these earlier codes have been developed in an essentially fixed environment as far as computer architecture is concerned, the next-generation code is likely to see a far more fluid environment. Therefore, in selecting a solution algorithm for a next-generation code, it is important to anticipate the computer architectures that are likely to become available over the next 10 to 20 years. The current CRAY computers achieve speeds in the range of 1 to 2 Gflops, while the 64-K Connection Machine has a peak speed of about 5 Gflops (64-bit precision). Several other massively parallel machines are under development which will use more powerful processors to achieve Teraflop speeds. Such machines would offer a 1,000-fold increase in speed over the current CRAY capabilities, provided that advantage could be taken of their parallel architectures. As noted in this report's introduction, such a gain in performance is expected to be necessary if the next-generation code is to achieve its ultimate computational objectives.

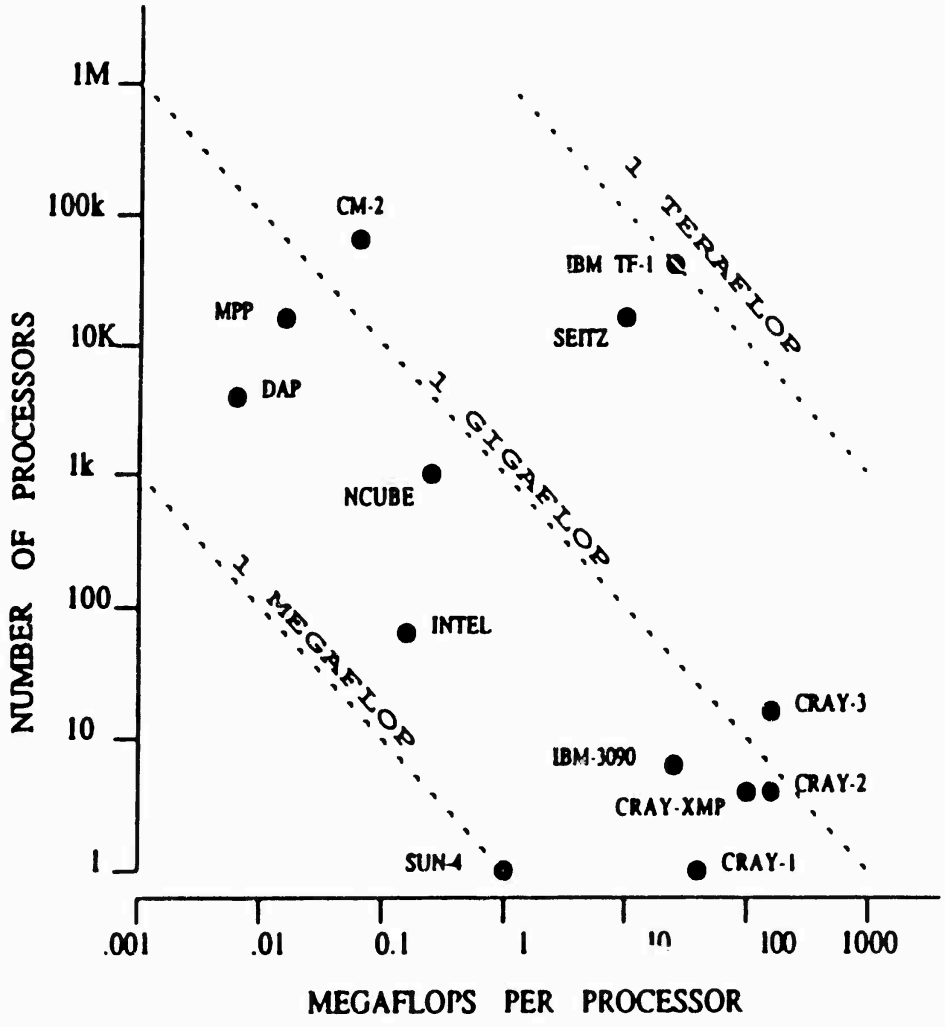

Figure 6. Performance comparisons of existing and planned computers (reference 52).

Particular interest has been focussed on the Connection Machine, a SIMD computer. Oran et al. [51] have compared the computational time per cell per step for two- and three-dimensional solutions of the Navier-Stokes equations using FCT on a CRAY-YMP processor and a 16-K Connection Machine. It was found that the Connection Machine was capable of running as much as five times faster than the CRAY, provided that simple boundary conditions were used. Long et al. [52] considered a time-marching method on the CRAY-XMP and on a 64-K Connection Machine. The Connection Machine was found to run 15 times faster than the CRAY if a structured mesh was used and to run at about the same speed if an

unstructured mesh was used. Jespersen and Levit [72] found the 16-K Connection Machine to be about two and a half times faster than the CRAY-XMP if an explicit solver was used and to be about the same if an implicit scheme was used. Considering that the CRAY-YMP is about twice as fast as the XMP, their finding is in line with that of Oran et al. [51]. These results strongly suggest that, in order to obtain maximum advantage of a SIMD machine, the solution method should be explicit and based on a structured mesh. This is not surprising since these two categories are predicated on local analysis of the flow and do not require information from remote processors. The same reasoning suggests that internal boundaries should be captured rather than represented explicitly if computational advantage is to be realized in a SIMD environment. Since the use of an implicit scheme or an unstructured mesh resulted in run times which were roughly equal on the CRAY and on the Connection Machine, a more open question might be whether there is a MIMD architecture for which the execution time is minimized for these categories of solution method. At the present time, according to Long et al. [52], current MIMD operating systems and compilers make them difficult to program in a manner significantly different from a SIMD operation. However, this area of investigation is undergoing vigorous development at the present time and improvements in both hardware and software are expected to emerge at a rapid pace. The prospect of a rapidly changing computer environment demands that the central flow solver be as simple as possible in order to promote ease of reprogramming on promising new systems. This requirement is completely compatible with the conclusion drawn from current experience with the SIMD architecture, namely, that the algorithm be explicit, based on a structured mesh, and that internal boundaries be captured.

With these desiderata in mind, let us recall the methods of solution which have been used to analyze the various types of propelling charge. All the codes used to model the SPG have used explicit solvers on structured meshes, except in instances when the tube wall boundary layer was of interest. This latter area has received relatively little attention due to the constitutive uncertainties and the difficulty of obtaining stable solutions. Some models have captured the charge increment boundaries. However, the models developed by Gough [11,14] have treated the increment boundaries explicitly and have, moreover, folded the properties of the increment containers into the internal boundary conditions. The codes used to model the RLPG have all been explicit and based on structured meshes. Internal boundaries have been captured. Finally, with regard to the ETCG, we have a full panoply of methods. However, we do note that at least one successful code has been based on an explicit solver, a structured mesh, and captured internal boundaries [44].

It, therefore, appears that a CFS which is explicit, uses a structured mesh, and captures internal boundaries can be applicable to the RLPG and the ETCG directly and also to a broad class of SPG designs. However, capturing the boundary of the charge increments is undesirable in our view since it leads to numerical diffusion of the propellant into the ambient ullage. In the next section, we will discuss a method of representation of the solid propellant which eliminates the possibility of diffusion of the propellant as effectively as an explicit representation of the internal boundary and, at the same time, allows the porosity to vary smoothly across the boundary.

4.4.2 Choice of Algorithms. We now outline the structure of the next-generation code in so far as it can be specified at the present time. We focus on specific attention on a choice of algorithms for a CFS to treat the continuous phase and certain of the discrete phases, and a large particle integrator (LPI) to treat those discrete phases which represent solid propellants. The present discussion should be viewed as proposing a course of development of the code and we, therefore, note uncertainties which can only be resolved by computational studies.

The structure of the code is illustrated schematically in Figures 7 and 8. Figure 7 serves mainly to relate the integration scheme to the ancillary code functions. Figure 8 focusses on the integration scheme per se. Figure 7 requires minimal discussion. We do indicate that the development of databases for the code should ultimately be supported by an artificial intelligence (AI) routine. Such a feature may not be necessary for initial code development studies in which databases are produced by individuals who are intimately familiar with the code structure and modeling assumptions as well as details of charge design. However, experience with previous codes suggests that the next-generation code will not be broadly useful unless a considerable degree of user-friendliness is built into the input routine.

We now turn to Figure 8. We note that the code may be viewed as having a main body which is the subject of initial development. This main body consists of the mesh algorithm, the CFS, the LPI, and the external boundary conditions. Included in the main body are subroutines to describe the continuous phase equation of state and kinetics and turbulence laws; the discrete phase equation of state and morphology and the phase interactions; the projectile motion, the plasma capillary (ETG), and the liquid propellant reservoir (RLPG); and, finally a model of the combustible cartridge case. This main body of coding is expected to address two- and three-dimensional details of all tank gun charges, with the exception of those which involve long unperforated sticks or packaging materials placed between increments. The main body should also address liquid propellant and ET artillery charges for which boundaries can be captured. Solid

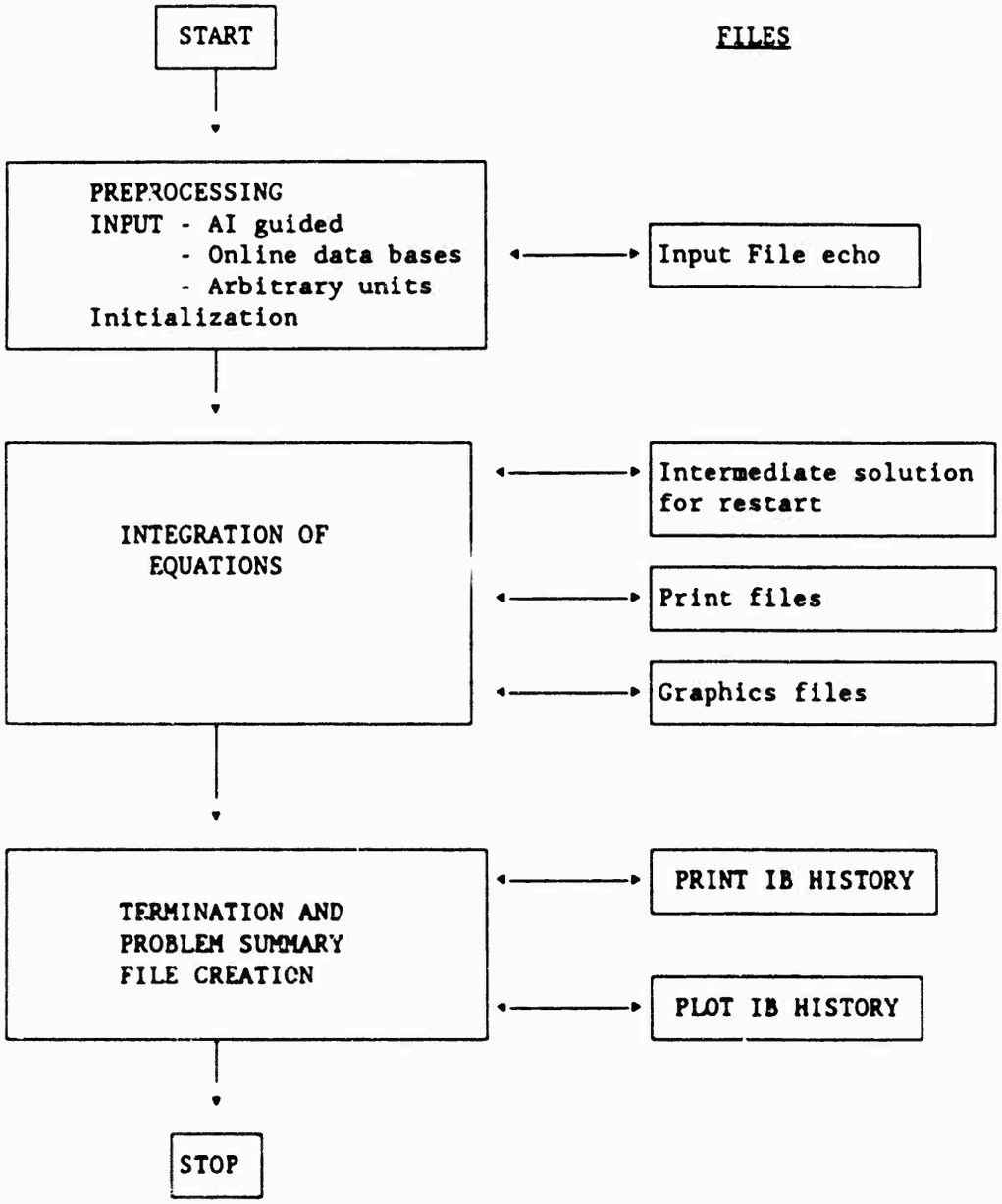

Figure 7. Overall structure of next-generation code.

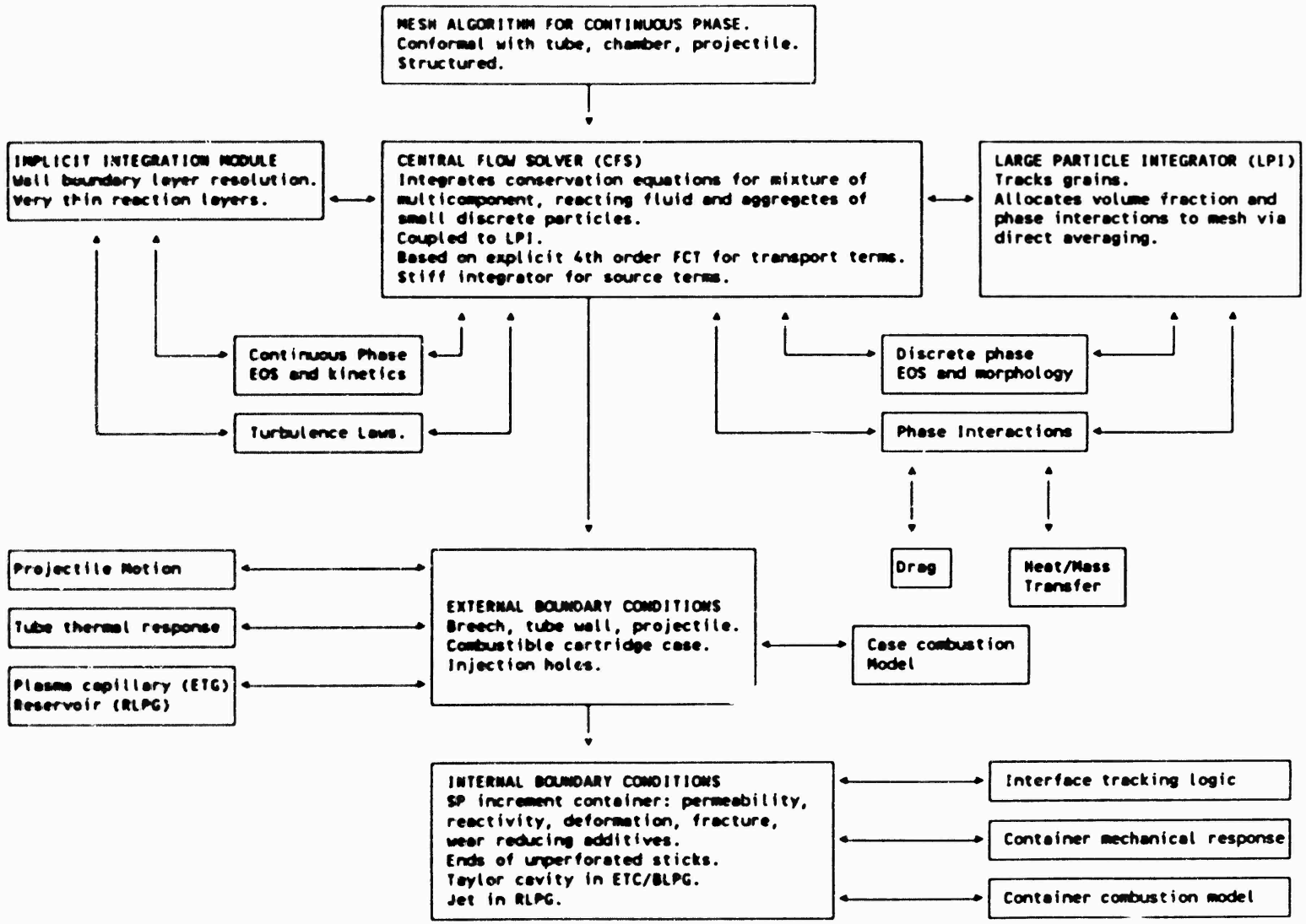

Figure 8. Stucture of integrating scheme for next-generation code.

propellant artillery charges will not be addressable by the main body since the internal boundary conditions due to the increment containers are of prime importance. A second stage of code development is envisaged in which modules are prepared to treat internal boundary conditions associated with increment containers, the ends of unperforated sticks, and explicit representations of the Taylor cavity in the ETCG or the injected jet of propellant in the RLPG. As shown in Figure 8, this supplementary body of coding will include interface tracking logic, the mechanical response of the increment containers, and a model of the combustion of the containers. The main body of coding is also not intended to address problems which involve the tube wall boundary layer or very thin reaction layers. For this class of problems, it is assumed that a separate implicit module will have to be written. Such a module would be supported by an analysis of the thermal response of the tube.

We now provide further discussion of the mesh algorithm, the CFS, and the LPI. Additional discussion of these topics, particularly the large particle integrator, can be found in reference 58.

In accordance with the conclusion of our general discussion, we use a structured mesh. The mesh is made conformal with the tube, the breechface, and the projectile base and afterbody. It is assumed that these constitute the external boundaries for the physical domain on which the solution is sought. Internal boundaries associated with shocks and contact discontinuities are captured and those associated with increment boundaries are smoothed by the large particle integrator. It is also assumed that fine details of the external boundaries can be neglected so that a regular structured mesh can be determined without an excessive number of mesh points and without boundary-induced distortion. As discussed in reference 58, we accommodate the presence of a long projectile afterbody and highly chambraged tubes by extending the mesh to include virtual cells. Mesh points are distributed over both the actual external boundaries and the virtual boundaries in a piecewise uniform manner. The use of virtual cells allows a regular labelling of all cells in the computational domain, thereby facilitating a direct map onto a massively parallel architecture. Virtual cells are simply ignored by the integration routine. Given the boundary distributions of the mesh points, the interior distributions follow readily from a standard equipotential mesh algorithm [73]. We note that mesh rezoning will be required from time to time if the chamber is highly chambraged or if there is an afterbody.

In previous work [11,14], we have elected to view the boundary of a solid propellant charge increment as a macroscopic surface of discontinuity. The surface was tracked explicitly and the mesh was made conformal with these explicit internal boundaries as well as the external boundaries. This had the result

that the structure of the increment boundary was propagated into the mesh distribution. Since a dispersed aggregate of particles can develop an arbitrary degree of deformation, numerical instability was found to occur in some instances. Increment boundary deformation led to mesh distortion which, in turn, led to numerical inaccuracy and subsequent to complete breakdown of the solution. In the present approach, the mesh is made conformal only with the inherently stable external boundaries so that this problem is eliminated.

The LPI performs a discretization of the solid propellant increments which is independent of the mesh on which the continuous phase is analyzed. In principle, it would be possible to represent a typical granular charge in terms of each of its individual grains since these are not especially numerous. In fact, in a three-dimensional calculation, one might have roughly 20,000 continuum mesh points and only about 1,000 propellant grains. However, the precise initial location of each of these grains is not known and, in any case, an averaging over the possible distributions is appropriate in the context of the macroscopic analysis. Accordingly, we represent the increment by a number of particles, each of which is weighted by a number density which relates it to a number of grains. The number density will not normally be an integer. In effect, we have a Lagrangian representation of the solid propellant. And, in fact, the integration of the equations of motion of the particles is performed in precisely the same way as in a coupled Lagrangian/Eulerian analysis. However, the continuity equation for the aggregate, equation 28, is not solved. Instead, the volume fraction is determined by a process of direct averaging over the aggregate.

An obvious method of averaging the properties of the aggregate would be to use the formal averages defined by equations 12 and 14. However, it would be necessary to make a specific choice of the weighting function g. Moreover, it is the case that if g is uniform over some sphere and zero elsewhere, the diameter of the sphere has to be quite large compared with the typical dimensions of the particles if the volume fraction is to be reasonably smooth. Celmins [74] has shown by direct calculation for aggregates of spheres that the averaging volume must contain of the order of 100 particles if the volume fraction is to be uniform to within 1%. The precise number depends on the packing of the spheres.

An averaging procedure which involves such a large number of particles is undesirable since it implies considerable computation at each mesh cell. Moreover, in a highly parallel environment, the procedure would either require an extensive template of particle properties to be stored at each mesh and updated from time to time, or it would require accessing data from remote processors. Apart from these

computational concerns, there is no obvious benefit to performing such a literal average over the aggregate. The macroscopic equations already imply that averaging has been performed and that details of the microflow have been incorporated in the interphase coupling terms. In the present application, we desire a simple process whereby the properties of the aggregate can be mapped onto the continuous phase computational grid in as local a manner as possible. We desire a method which yields a completely uniform volume fraction over the interior of the aggregate when it is packed uniformly. At the boundaries, we desire that the volume fraction drop to zero over a length comparable to the scale of heterogeneity. Such a method would produce a continuous distribution of porosity everywhere throughout the physical domain. The increment boundaries would not correspond to discontinuities but rather to zones of large but finite porosity gradients. The properties of the continuous phase would likewise vary strongly but continuously as one crossed the increment boundary.

We illustrate such a simple method by reference to a one-dimensional problem. Consider an array of particles each having volume $V_{p_i} n_i$ where V_{p_i} is the volume of an individual grain and n_i is the number of grains corresponding to the i-th particle. Let the coordinates of the particles be x_i. Then the i-th particle is assigned a volume fraction distribution $\epsilon_i(x)$ such that

$$\alpha_i(x) = \begin{cases} a_i f\left(\dfrac{x_i - x}{x_i - x_{i-1}}\right) & , \quad x_{i-1} \le x \le x_i \\ a_i f\left(\dfrac{x - x_i}{x_{i+1} - x_i}\right) & , \quad x_i \le x \le x_{i+1} \end{cases} . \tag{45}$$

A simple choice for f is that it be linear and homogeneous. Then a_i is determined from the condition

$$n_i V_{p_i} = \int_{x_{i-1}}^{x_{i+1}} \alpha_i(x)\,dx . \tag{46}$$

In the interval $x_i \le x \le x_{i+1}$, the total volume fraction of the aggregate is resolved as the sum of the contributions of the particles at the bounding locations. It is easy to verify that for uniformly spaced and

equally weighted particles, this leads to a uniform distribution as desired. Moreover, at the boundaries, one has contributions from only one side. Accordingly, the volume fraction drops to zero linearly at the boundaries. When the array is nonuniform, the choice of a linear dependence for f yields a porosity distribution that is continuous but only piecewise differentiable. A cubic dependence for f can be shown to yield a porosity distribution for which the first derivative is also continuous. Higher order derivatives can be made continuous by using higher order polynomials of odd order to represent the dependence of f [58]. Other properties of the aggregate can be averaged in an analogous manner. For multidimensional problems, products of the distribution functions lead to averaging of the particle properties over a characteristic cell.

In one-dimensional flow, the choice of the cell for each particle is determined uniquely by its neighbors. In multi-dimensional flows, there is some ambiguity once the initial regularity of the aggregate array is lost. Numerical experiments are required to determine the best strategies for cell definition. It is also of interest to determine whether a linear or a cubic distribution for f is better. Higher order distributions are not likely to be of interest. The choice of the distribution for f will be strongly influenced by the properties of the CFS, specifically the resolution of the strong gradients near the boundaries of the aggregate. Finally, since the foregoing procedure involves interpolation back and forth between the particle array and the continuum mesh, it will be important to determine the computational penalty, particularly in a massively parallel environment.

We now consider the choice of integration algorithm for the CFS. The CFS is intended to integrate the balance equations for the continuous phase as well as those for those discrete phases which consist of small, continuously distributed particles or droplets. Accordingly, the CFS is intended to integrate all the balance equations in the case of simulations of the RLPG or the ETCG. The LPI is intended to address charge increments for the SPG. It is possible, of course, that designs of the ETCG could be advanced in which the plasma is injected into a granular propellant. In such a case, the LPI would presumably be activated. In practice, we expect the code user to be able to designate each discrete phase as addressable by either the LPI or the CFS. In addition, we expect the user to be able to designate certain of the discrete phases as being in mechanical or thermal equilibrium with the continuous phase. Such conditions eliminate the need to specify the interphase drag or heat transfer and are appropriate when the particles or droplets are sufficiently small or when the morphology is poorly characterized.

As we have already mentioned, we favor the use of the fourth-order FCT algorithm described by Oran and Boris [29] as the basis for the CFS. The Riemann solvers [26,27,75] would also be favored candidates, with that due to Roe [75] being preferred to the version of van Leer [26,27] on the basis of the findings of Ridder and Beddini [76], if the code were to be applied exclusively to problems in which solid propellants were not a consideration. By their very nature, Riemann-based solvers do an excellent job of capturing shocks and contact discontinuities. However, as noted by Oran [29], fourth-order FCT performs acceptably in a shock tube test case even though it is not predicated on the characteristic structure of the equations. Moreover, for pure convection, fourth-order FCT performs better than the Riemann solvers. Since the presence of solid propellant charge increments will impose large gradients on the state variables which are uncorrelated with the characteristic structure of the balance equations, the Riemann-based solvers are not expected to offer any advantage and the simpler FCT approach is to be preferred.

We also note that FCT has been used successfully for one model of the ETCG [44]. Moreover, it has been applied successfully to simulations of DDT in porous explosives [77], a problem related to that of flamespreading in granular propellants, but involving much greater numerical strain due to the stiffness of the phase interaction and chemical reaction terms.

It is expected that computational tests will be required to verify the ability of FCT to cope with the gradients at the solid propellant increment boundaries. Moreover, there are ambiguities in the multi-dimensional formulation of FCT and in the coordination of the flux-limiting of several variables which will need to be resolved.

We conclude with some comments on internal boundary conditions. The use of direct averaging of the aggregate properties is intended to eliminate the representation of the mixture boundary as a discontinuity. This will facilitate the solution of solid propellant charge problems since a structured mesh can easily be established to accommodate the configuration of the external boundaries, even if the projectile has a long afterbody. However, there is no escaping the difficulties of representing the properties of the container. As a minimum, the permeability and reactivity of the container must be imposed as internal boundary conditions until such time as the container has fully ruptured. Subsequently, it can be converted to an aggregate of particles.

The approach used in the PISCES Code [25] is presently thought to be the best way to represent the container properties. The container can be taken to move independently of the propellant or to be tied to the mixture boundary as in TDNOVA [14]. The finite volume analysis in the flow solver is required to note the partial or complete occlusion of a normal computational cell and to impose the appropriate internal boundary conditions on the fluid/structure interfaces.

It also appears that perforated sticks will require the consideration of internal boundary conditions in order to couple the flow in the perforations to that in the interstices. A Taylor cavity of the type discussed by Chen [39] also constitutes an explicit internal boundary.

5. REFERENCES

1. Corner, J. Theory of the Interior Ballistics of Guns. NY: Wiley, 1950.

2. Kent, R. H. "Study of Ignition of 155-mm Gun." Report 22, U.S. Army Ballistic Research Laboratory, Aberdeen Proving Ground, MD, 1935.

3. Hedden, S. E., and G. A. Nance. "An Experimental Study of Pressure Waves in Gun Chambers." Report 1534, Naval Proving Ground, 1957.

4. Budka, A. J., and J. D. Knapton. "Pressure Wave Generation in Gun Systems—A Survey." BRL-MR-2567, U.S. Army Ballistic Research Laboratory, Aberdeen Proving Ground, MD, 1975.

5. May, I. W., and A. W. Horst. "Charge Design Considerations and Their Effects on Pressure Waves in Guns." Interior Ballistics of Guns, Progress in Astronautics and Aeronautics, vol. 66, edited by H. Krier and M. Summerfield, 1979.

6. Baer, P. G., and J. M. Frankle. "Study of Ignition of 155-mm Gun." BRL-Report 1183, U.S. Army Ballistic Research Laboratory, Aberdeen Proving Ground, MD, 1962.

7. Fisher, E. B., and K. W. Graves. "Mathematical Model of Double Base Propellant and Ignition in the 81-mm Mortar." Calspan Report DG-3029-D-1, 1972.

8. Gough, P. S., and F. J. Zwarts. "Theoretical Model for Ignition of Gun Propellant." Report SRC-R-67, Space Research Corporation, 1972.

9. East, J. L., and D. R. McClure. "Projectile Motion Predicted by a Solid/Gas Flow Interior Ballistic Model." Proceedings of the 10th JANNAF Combustion Meeting, 1973.

10. Krier, H., W. F. van Tassell, S. Rajan, and J. Vershaw. "Model of Flamespreading and Combustion Through Packed Beds of Propellant Grains." TR-AAE74-1, University of Illinois at Urbana-Champaign, 1974.

11. Gough, P. S. "The XNOVAKTC Code." Report PGA-TR-86-1, Paul Gough Associates, 1986.

12. Morrison, W. F., J. D. Knapton, and G. Klingenberg. "Liquid Propellants for Gun Applications." Proceedings of the 7th International Ballistics Symposium, 1983.

13. Juhasz, A. A., K. Jamison, K. White, and G. Wren. "Introduction to Electrothermal Gun Propulsion." CPIA Publication 498, vol. IV, pp. 223-244, 1988.

14. Gough, P. S. "Modeling of Rigidized Gun Propelling Charges." BRL-CR-00518, U.S. Army Ballistic Report Laboratory, Aberdeen Proving Ground, MD, 1983.

15. Meinecke, E., and R. Heiser. "A Complete Numerical Solution of the Interior Ballistics Chambrage Problem." Proceedings of the 11th International Symposium on Ballistics, 1989.

16. Groenenboom, P. H. L., and P. Thomsen. "Two Phase Flow Computation for a 40-mm Granular Propellant Gun in Comparison with Experimental Results." Proceedings of the 11th International Symposium on Ballistics, 1989.

17. Fitt, A. D., A. B. Crowley, J. A. G. Aston, and E. F. Toro. "Contrasting Numerical Methods for Two-Dimensional Two-Phase Interior Ballistic Flows." Proceedings of the 11th International Symposium on Ballistics, 1989.

18. Gibeling, H. J., and H. McDonald. "An Implicit Numerical Analysis for Two-Dimensional Turbulent Interior Ballistic Flows." BRL-CR-00523, U.S. Army Ballistic Research Laboratory, Aberdeen Proving Ground, MD, 1984.

19. Schmitt, J. A. "A Numerical Algorithm for the Multidimensional, Multiphase, Viscous Equations of Interior Ballistics." Proceedings of the 2nd Army Conference on Applied Mathematics and Computing, 1984.

20. MacCormack, R. W. "The Effect of Viscosity in Hypervelocity Impact Cratering." AIAA Paper No. 69–354, 1969.

21. Gough, P. S. "Numerical Simulation of Current Artillery Charges Using the TDNOVA Code." PGA-TR-85-1, Paul Gough Associates, 1985.

22. Gough, P. S. "Enhanced Interior Ballistics Codes." PGA-TR-91-2, Paul Gough Associates, 1991.

23. Gough, P. S. "Effect of Charge Geometry on Tube Wall Boundary Layer." Proceedings of the 27th JANNAF Combustion Meeting, 1990.

24. Briley, W. R., and H. McDonald. "Solution of the Multidimensional Compressible Navier-Stokes Equations by a Generalized Implicit Method." Journal of Computational Physics, vol. 24, no. 4, pp. 372–397, 1977.

25. "PISCES-2DELK User's Manual." PISCES International B. V., The Netherlands, Undated.

26. Van Leer, B. "Towards the Ultimate Conservative Difference Scheme. IV. A New Approach to Numerical Convection." Journal of Computational Physics, vol. 23, pp. 276–299, 1977.

27. Van Leer, B. "Towards the Ultimate Conservative Difference Scheme. V. A Second Order Sequel to Godunov's Method." Journal of Computational Physics, vol. 32, pp. 101–136, 1979.

28. Groenenboom, P. H. L. "Equations and Numerical Solution of Gas-Particle Flow. GRAINS level 26." TR-87-2118/1, PISCES International BV, 1987.

29. Oran, E. S., and J. P. Boris. Numerical Simulation of Reactive Flow. Elsevier, 1987.

30. Gough, P. S. "Review of GE Model of Regenerative Liquid Propellant Gun." Paul Gough Associates, 1977.

31. Pagan, G., A. Harvey, and D. C. A. Izod. "Regenerative Liquid Propellant Gun Modeling." Proceedings of the 7th International Ballistics Symposium, 1983.

32. Coffee, T. P. "A Lumped Parameter Code for Regenerative Liquid Propellant Guns." BRL-TR-2703, U.S. Army Ballistic Research Laboratory, Aberdeen Proving Ground, MD, 1985.

33. Gough, P. S. "Continuum Modeling of Regenerative Liquid Propellant Guns and Hybrid Traveling Charge Systems." BRL-CR-624, U.S. Army Ballistic Research Laboratory, Aberdeen Proving Ground, MD, 1989.

34. Heiser, R. "Interior Ballistic Modeling of Regenerative Liquid Propellant Guns in a Gas Dynamic Model." Proceedings of the 10th International Symposium on Ballistics, 1987.

35. Steffens, U., D. Krassin, and R. Rittel. "Two-Phase Flow Predictions of Regenerative Liquid Propulsion-A Comparison with Experimental Results." Proceedings of the 10th International Symposium on Ballistics, 1987.

36. Steffens, U., R. Rittel., and K. Florie. "Applications of a Three-Dimensional Gasdynamic Simulation Model to Interior Ballistics." Proceedings of the 11th International Symposium on Ballistics, 1989.

37. Coffee, T. P. "A Two-Dimensional Model for the Combustion Chamber/Gun Tube of a Concept VI C Regenerative Liquid Propellant Gun." Proceedings of the 27th JANNAF Combustion Meeting, 1990.

38. Kuo, K. K., F. B. Cheung, and J. L. Chen. "A Multi-Phase Multi-Dimensional Transient Bulk-Loaded Liquid Propellant Gun Model." Proceedings of the 11th International Symposium on Ballistics, 1989.

39. Chen, J. L., K. K. Kuo, and F. B. Cheung. "Theoretical Modeling of the Interior Ballistic Processes in an Electrothermal Gun." Proceedings of the 27th JANNAF Combustion Meeting, 1990.

40. Kashiwa, B. A., N. T. Padial, and D. Butler. "Toward a Comprehensive Model for Electrothermal Gun Performance." Proceedings of the 27th JANNAF Combustion Meeting, 1990.

41. Cook, D. C., J. A. Dyvik, and G. S. Chryssomallis. "A Multidimensional Electrothermal Model." Proceedings of the 26th JANNAF Combustion Meeting, 1989.

42. Winsor, N. K., and S. A. Goldstein. "Finite Element Modeling of an Electrothermal Gun." Proceedings of the 27th JANNAF Combustion Meeting, 1990.

43. Sinha, N., A. Hosangadi, and S. M. Dash. "Development of an Upwind/Implicit Computational Model for the Advancement of Army ETC Guns." JANNAF Workshop on ETC Modeling and Diagnostics, 1991.

44. Hsiao, C. C., G. Phillips, and F. Su. "First Principles Modeling of a DNA 60mm ETC Gun Design." JANNAF Workshop on ETC Modeling and Diagnostics, 1991.

45. Patanker, S. V., and D. B. Spalding. "A Calculation Procedure for Heat, Mass and Momentum Transfer in Three-Dimensional Parabolic Flows." Int. Journal of Heat and Mass Transfer, vol. 15, pp. 1787--1806, 1972.

46. Peaceman, D. W., and H. H. Rachford. "The Numerical Solution of Parabolic and Elliptic Differential Equations." J. Society Industrial and Applied Mathematics, vol. 3, no. 1, pp. 28–41, 1955.

47. Löhner, R., K. Morgan, J. Peraire, M. Vahdati. "Finite Element Flux-Corrected Transport (FEM-FCT) for the Euler and Navier-Stokes Equations." Int. J. of Num. Meth. Fluids, vol. 7, p. 093, 1987.

48. Williams, F. A. Combustion Theory. Addison-Wesley, 1965.

49. Kuo, K. K. Principles of Combustion. John Wiley and Sons, 1986.

50. Gough, P. S. "Extensions to NOVA Flamespread Modeling Capacity." PGA-TR-81-2, 1981.

51. Oran, E. S., J. P. Boris, and E. F. Brown. "Fluid-Dynamic Computations on a Connection Machine—Preliminary Timings and Complex Boundary Conditions." AIAA Paper 90-0335, 1990.

52. Long, L. N., M. M. S. Khan, and H. T. Sharp. "Massively Parallel Three-Dimensional Euler/Navier-Stokes Method." AIAA Journal, vol. 29, no. 5, pp. 657–666, 1991.

53. Richtmyer, R. D., and K. W. Morton. "Difference Methods for Initial Value Problems." Interscience, 1967.

54. Drew, D. A. "Averaged Field Equations for Two-Phase Media." Stud. Appl. Math., vol. L, no. 2, pp.133–166, 1971.

55. Gough, P. S. "The Flow of a Compressible Gas Through an Aggregate of Mobile Reacting Particles." Ph.D. Thesis, Department of Mechanical Engineering, McGill University, Montreal, Canada, 1974.

56. Ishii, M. "Thermo-Fluid Dynamic Theory of Two-Phase Flow." Eyrolles, Paris, 1975.

57. Gough, P. S. "On the Closure and Character of the Balance Equations for Heterogeneous Two-Phase Flow." Dynamics and Modelling of Reactive Systems, edited by W. E. Stewart, W. H. Ray, and C. C. Conley, Academic Press, 1980.

58. Gough, P. S. "Feasibility Study for Three-Dimensional Interior Ballistic Code." PGA-TR-92-1, 1992.

59. O'Rourke, P. J., and F. V. Bracco. "Modeling of Drop Interactions in Thick Sprays and a Comparison with Experiments." The Institution of Mechanical Engineers, Publication 1980-9, 1980.

60. Zeldovitch, Ya. B., and Yu. P. Raizer. Physics of Shock Waves and High Temperature Hydrodynamic Phenomena. Academic Press, 1966.

61. Garloff, J., and R. Heiser. "Comparison of Two Algebraic Eddy Viscosity Models for Turbulent Modeling of Interior Ballistic Flows." Ernst-Mach-Institut, Report 7/88, 1988.

62. Garloff, J.,and R. Heiser. "Turbulence Modeling of One-Phase Interior Ballistics Flows by a Two-Equation Model." Ernst-Mach-Institut, Report 1/88, 1988.

63. Hinze, J. O. Turbulence. McGraw-Hill, 1959.

64. Freedman, E. "BLAKE—A Thermodynamic Code Based on TIGER: Users' Guide and Manual." BRL-TR-02411, U.S. Army Ballistic Research Laboratory, Aberdeen Proving Ground, MD, 1982.

65. Su, F. Y., and M. J. Stock. "Real Equations of State for Two-Phase Flow Electrothermal Chemical Gun Application." Proceedings of the 28th JANNAF Combustion Meeting, 1991.

66. Kooker, D. E. "Modeling of Compaction Wave Behavior in confined Granular Energetic Material." BRL-TR-3138, U.S. Army Ballistic Research Laboratory, Aberdeen Proving Ground, MD, 1990.

67. Coffee, T. P., P. G. Baer, W. F. Morrison, and G. P. Wren. "Jet Breakup and Combustion Modeling for the Regenerative Liquid Propellant Gun." BRL-TR-3223, U.S. Army Ballistic Research Laboratory, Aberdeen Proving Ground, MD, 1991.

68. Buckingham, A. C. "Propellant Driven Turbulent Interior Ballistics and Wall Erosion." AIAA Paper 79-0007, 17th Aerospace Sciences Meeting, 1979.

69. Dukowicz, J. K. "A Particle-Fluid Numerical Model for Liquid Sprays." Journal of Computational Physics, vol. 35, p. 229, 1980.

70. Chen, J-L. "A Theoretical and Experimental Study of the Interior Ballistic Processes of an Electrothermal Gun." Ph.D. Thesis, Department of Mechanical Engineering, Pennsylvania State University, 1990.

71. Gough, P. S. "Theoretical Modeling of Navy Propelling Charges." PGA-TR-84-1, 1984.

72. Jespersen, D. C., and C. Levit. "A Computational Fluid Dynamics Algorithm on a Massively Parallel Computer." AIAA Paper 89-1936-CP, 1989.

73. Thompson, J. F., F. C. Thames, and C. W. Mastin. "Automatic Numerical Generation of Body-Fitted Curvilinear Coordinate Systems for Field Containing Any Number of Arbitrary Two-Dimensional Bodies." Journal Computational Physics, vol. 15, p. 299, 1974.

74. Celmins, A. K. R. "Averaging Effects in Models of Three-Dimensional Two-Phase Flows." BRL-TR-2598, U.S. Army Ballistic Research Laboratory, Aberdeen Proving Ground, MD, 1984.

75. Roe, P. L. "Approximate Riemann Solvers, Parameter Vectors, and Difference Schemes." Journal Computational Physics, vol. 43, pp. 357–372, 1981.

76. Ridder, J. P., and R. A. Beddini. "A Time Accurate Finite Volume Method for Propulsion Chamber Flows." Proceedings of the 25th Joint Propulsion Conference, AIAA Paper 89-2554, 1989.

77. Gross, R. J., and M. R. Baer. "A Study of Numerical Solution Methods for Two-Phase Flows." Sandia Report SAND 87-1633, 1986.

INTENTIONALLY LEFT BLANK.

NOMENCLATURE

A_i	Bounding surface of i-th phase
b	Covolume
C_μ	Turbulence parameter
c_p	Specific heat at constant pressure
c_v	Specific heat at constant volume
D	Diffusivity
e	Internal energy
f_{d_i}	Drag on i-th discrete phase
g	Weighting function
h_{i_o}	Heat of formation of i-th species
$\mathbf{I}$	Unit tensor
k	Turbulent kinetic energy
$\dot{m}_{d_i}$	Rate of decomposition of i-th discrete phase
N_c	Number of species in continuous phase
N_d	Number of discrete phases
n_{d_i}	Number density of i-th discrete phase
$\mathbf{n}$	Unit normal vector
p	Pressure
$\mathbf{q}$	Heat flux vector
q_{d_i}	Heat flux to surface of i-th discrete phase
R	Gas constant
$\dot{r}_{d_i}$	Rate of surface regression of i-th discrete phase
S_{d_i}	Surface area of i-th discrete phase particle or droplet

S_i	Surface area per unit volume of i-th phase
T	Temperature of continuous phase
T_{d_i}	Temperature of i-th discrete phase
t	Time
$\mathbf{u}$	Velocity of continuous phase
$\mathbf{u}_{d_i}$	Velocity of i-th discrete phase
V_{d_i}	Volume of i-th discrete phase particle or droplet
V_i	Volume of i-th phase
$\mathbf{v}_i$	Diffusion velocity of i-th species of continuous phase
$\mathbf{w}$	Boundary velocity
X_i	Mole fraction of i-th species of continuous phase
$\mathbf{x}$	Position vector
Y_i	Mass fraction of i-th species of continuous phase
$Y_{d_{ij}}$	Mass fraction of j-th species of continuous phase produced by decomposition of i-th discrete phase
$\mathbf{y}$	Dummy position vector

GREEK SYMBOLS

α_i	Volume fraction of i-th phase
α_{d_i}	Volume fraction of i-th discrete phase
α_R	Rosseland mean absorption coefficient
ε	Rate of dissipation of turbulent kinetic energy
λ	Thermal conductivity
μ	Molecular viscosity
μ'	Bulk viscosity

μ_T	Turbulent viscosity
ρ	Density of continuous phase
ρ_{d_i}	Density of i-th discrete phase
σ	Stress tensor for continuous phase
σ_{d_i}	Stress tensor for i-th discrete phase
σ	Stephan-Boltzman constant
τ	Stress deviator
τ	Dummy time variable
$\dot{\omega}_i$	Rate of i-th reaction in continuous phase
$\dot{\omega}_{s_i}$	Rate of production of i-th species of continuous phase at surface

INTENTIONALLY LEFT BLANK.

No. of Copies	Organization
2	Administrator Defense Technical Info Center ATTN: DTIC-DDA Cameron Station Alexandria, VA 22304-6145
1	Commander U.S. Army Materiel Command ATTN: AMCAM 5001 Eisenhower Ave. Alexandria, VA 22333-0001
1	Director U.S. Army Research Laboratory ATTN: AMSRL-OP-CI-AD, Tech Publishing 2800 Powder Mill Rd. Adelphi, MD 20783-1145
1	Director U.S. Army Research Laboratory ATTN: AMSRL-OP-CI-AD, Records Management 2800 Powder Mill Rd. Adelphi, MD 20783-1145
2	Commander U.S. Army Armament Research, Development, and Engineering Center ATTN: SMCAR-IMI-I Picatinny Arsenal, NJ 07806-5000
2	Commander U.S. Army Armament Research, Development, and Engineering Center ATTN: SMCAR-TDC Picatinny Arsenal, NJ 07806-5000
1	Director Benet Weapons Laboratory U.S. Army Armament Research, Development, and Engineering Center ATTN: SMCAR-CCB-TL Watervliet, NY 12189-4050
1	Director U.S. Army Advanced Systems Research and Analysis Office (ATCOM) ATTN: AMSAT-R-NR, M/S 219-1 Ames Research Center Moffett Field, CA 94035-1000

No. of Copies	Organization
1	Commander U.S. Army Missile Command ATTN: AMSMI-RD-CS-R (DOC) Redstone Arsenal, AL 35898-5010
1	Commander U.S. Army Tank-Automotive Command ATTN: AMSTA-JSK (Armor Eng. Br.) Warren, MI 48397-5000
1	Director U.S. Army TRADOC Analysis Command ATTN: ATRC-WSR White Sands Missile Range, NM 88002-5502
(Class. only) 1	Commandant U.S. Army Infantry School ATTN: ATSH-CD (Security Mgr.) Fort Benning, GA 31905-5660
(Unclass. only) 1	Commandant U.S. Army Infantry School ATTN: ATSH-WCB-O Fort Benning, GA 31905-5000
1	WL/MNOI Eglin AFB, FL 32542-5000
	Aberdeen Proving Ground
2	Dir, USAMSAA ATTN: AMXSY-D AMXSY-MP, H. Cohen
1	Cdr, USATECOM ATTN: AMSTE-TC
1	Dir, ERDEC ATTN: SCBRD-RT
1	Cdr, CBDA ATTN: AMSCB-CII
1	Dir, USARL ATTN: AMSRL-SL-I
10	Dir, USARL ATTN: AMSRL-OP-CI-B (Tech Lib)

No. of Copies	Organization
1	Chairman DOD Explosives Safety Board Room 856-C Hoffman Bldg. 1 2461 Eisenhower Avenue Alexandria, VA 22331-0600
1	Headquarters U.S. Army Materiel Command ATTN: AMCICP-AD, M. Fisette 5001 Eisenhower Ave. Alexandria, VA 22333-0001
1	U.S. Army Ballistic Missile Defense Systems Command Advanced Technology Center P.O. Box 1500 Huntsville, AL 35807-3801
1	Department of the Army Office of the Product Manager 155mm Howitzer, M109A6, Paladin ATTN: SFAE-AR-HIP-IP, Mr. R. De Kleine Picatinny Arsenal, NJ 07806-5000
3	Project Manager Advanced Field Artillery System ATTN: SFAE-ASM-AF-E, LTC A. Ellis T. Kuriata J. Shields Picatinny Arsenal, NJ 07801-5000
1	Project Manager Advanced Field Artillery System ATTN: SFAE-ASM-AF-Q, W. Warren Picatinny Arsenal, NJ 07801-5000
2	Commander Production Base Modernization Agency U.S. Army Armament Research, Development, and Engineering Center ATTN: AMSMC-PBM, A. Siklosi AMSMC-PBM-E, L. Laibson Picatinny Arsenal, NJ 07806-5000
4	PEO-Armaments Project Manager Tank Main Armament System ATTN: AMCPM-TMA AMCPM-TMA-105 AMCPM-TMA-120 AMCPM-TMA-AS, H. Yuen Picatinny Arsenal, NJ 07806-5000
	Commander U.S. Army Armament Research, Development, and Engineering Center ATTN: SMCAR-CCH-V, C. Mandala E. Fennell SMCAR-CCH-T, L. Rosendorf SMCAR-CCS Picatinny Arsenal, NJ 07806-5000
19	Commander U.S. Army Armament Research, Development, and Engineering Center ATTN: SMCAR-AEE, J. Lannon SMCAR-AEE-B, A. Beardell D. Downs S. Einstein S. Westley S. Bernstein J. Rutkowski B. Brodman P. O'Reilly R. Cirincione A. Grabowsky P. Hui J. O'Reilly SMCAR-AEE-WW, M. Mezger J. Pinto D. Wiegand P. Lu C. Hu SMCAR-AES, S. Kaplowitz Picatinny Arsenal, NJ 07806-5000
1	Commander U.S. Army Armament Research, Development and Engineering Center ATTN: SMCAR-HFM, E. Barrieres Picatinny Arsenal, NJ 07806-5000

No. of Copies	Organization
9	Commander U.S. Army Armament Research, Development and Engineering Center ATTN: SMCAR-FSA-F, LTC R. Riddle SMCAR-FSC, G. Ferdinand SMCAR-FS, T. Gora SMCAR-FS-DH, J. Feneck SMCAR-FSS-A, R. Kopmann B. Machek L. Pinder SMCAR-FSN-N, K. Chung Picatinny Arsenal, NJ 07806-5000
3	Director Benet Weapons Laboratories ATTN: SMCAR-CCB-RA, G.P. O'Hara G.A. Pflegl SMCAR-CCB-S, F. Heiser Watervliet, NY 12189-4050
2	Commander U.S. Army Research Office ATTN: Technical Library D. Mann P.O. Box 12211 Research Triangle Park, NC 27709-2211
1	Director Army Research Office ATTN: AMXRO-MCS, Mr. K. Clark P.O. Box 12211 Research Triangle Park, NC 27709-2211
1	Director Army Research Office ATTN: AMXRO-RT-IP, Library Services P.O. Box 12211 Research Triangle Park, NC 27709-2211
1	Commander, USACECOM R&D Technical Library ATTN: ASQNC-ELC-IS-L-R, Myer Center Fort Monmouth, NJ 07703-5301
1	Commandant U.S. Army Aviation School ATTN: Aviation Agency Fort Rucker, AL 36360

No. of Copies	Organization
1	Program Manager U.S. Tank-Automotive Command ATTN: AMCPM-ABMS, T. Dean Warren, MI 48092-2498
1	Project Manager U.S. Tank-Automotive Command Fighting Vehicle Systems ATTN: SFAE-ASM-BV Warren, MI 48397-5000
1	Project Manager, Abrams Tank System ATTN: SFAE-ASM-AB Warren, MI 48397-5000
1	Director HQ, TRAC RPD ATTN: ATCD-MA Fort Monroe, VA 23651-5143
1	Commander U.S. Army Belvoir Research and Development Center ATTN: STRBE-WC Fort Belvoir, VA 22060-5006
1	Director U.S. Army TRAC-Ft. Lee ATTN: ATRC-L, Mr. Cameron Fort Lee, VA 23801-6140
1	Commandant U.S. Army Command and General Staff College Fort Leavenworth, KS 66027
1	Commandant U.S. Army Special Warfare School ATTN. Rev and Trng Lit Div Fort Bragg, NC 28307
1	Commander Radford Army Ammunition Plant ATTN: SMCAR-QA/HI LIB Radford, VA 24141-0298

No. of Copies	Organization
1	Commander U.S. Army Foreign Science and Technology Center ATTN: AMXST-MC-3 220 Seventh Street, NE Charlottesville, VA 22901-5396
2	Commandant U.S. Army Field Artillery Center and School ATTN: ATSF-CO-MW, E. Dublisky ATSF-CN, P. Gross Ft. Sill, OK 73503-5600
1	Commandant U.S. Army Armor School ATTN: ATZK-CD-MS, M. Falkovitch Armor Agency Fort Knox, KY 40121-5215
1	U.S. Army European Research Office ATTN: USARDSG-UK Dr. Roy E. Richenbach Box 65 FPO New York 09510-1500
2	Commander Naval Sea Systems Command ATTN: SEA 62R SEA 64 Washington, DC 20362-5101
1	Commander Naval Air Systems Command ATTN: AIR-954-Tech Library Washington, DC 20360
4	Commander Naval Research Laboratory ATTN: Technical Library Code 4410, K. Kailasanate J. Boris E. Oran Washington, DC 20375-5000
1	Office of Naval Research ATTN: Code 473, R.S. Miller 800 N. Quincy Street Arlington, VA 22217-9999

No. of Copies	Organization
1	Office of Naval Technology ATTN: ONT-213, D. Siegel 800 N. Quincy St. Arlington, VA 22217-5000
2	Commander Naval Surface Warfare Center ATTN: Code 730 Code R-13, R. Bernecker Silver Spring, MD 20903-5000
7	Commander Naval Surface Warfare Center ATTN: T.C. Smith K. Rice S. Mitchell S. Peters J. Consaga C. Gotzmer Technical Library Indian Head, MD 20640-5000
4	Commander Naval Surface Warfare Center ATTN: Code G30, Guns & Munitions Div Code G32, Guns Systems Div Code G33, T. Doran Code E23 Technical Library Dahlgren, VA 22448-5000
5	Commander Naval Air Warfare Center ATTN: Code 388, C.F. Price T. Boggs Code 3895, T. Parr R. Derr Information Science Division China Lake, CA 93555-6001
1	Commanding Officer Naval Underwater Systems Center ATTN: Code 5B331, Technical Library Newport, RI 02840
1	AFOSR/NA ATTN: J. Tishkoff Bolling AFB, D.C. 20332-6448

No. of Copies	Organization
1	OLAC PL/TSTL ATTN: D. Shiplett Edwards AFB, CA 93523-5000
3	AL/LSCF ATTN: J. Levine L. Quinn T. Edwards Edwards AFB, CA 93523-5000
1	WL/MNAA ATTN: B. Simpson Eglin AFB, FL 32542-5434
1	WL/MNME Energetic Materials Branch 2306 Perimeter Rd. STE 9 Eglin AFB, FL 32542-5910
1	WL/MNSH ATTN: R. Drabczuk Eglin AFB, FL 32542-5434
2	NASA Langley Research Center ATTN: M.S. 408, W. Scallion D. Witcofski Hampton, VA 23605
1	Central Intelligence Agency Office of the Central References Dissemination Branch Room GE-47, HQS Washington, DC 20502
1	Central Intelligence Agency ATTN: J. Backofen NHB, Room 5N01 Washington, DC 20505
1	SDIO/TNI ATTN: L.H. Caveny Pentagon Washington, DC 20301-7100
1	SDIO/DA ATTN: E. Gerry Pentagon Washington, DC 21301-7100

No. of Copies	Organization
2	HQ DNA ATTN: D. Lewis A. Fahey 6801 Telegraph Rd. Alexandria, VA 22310-3398
1	Director Sandia National Laboratories Energetic Materials & Fluid Mechanics Department, 1512 ATTN: M. Baer P.O. Box 5800 Albuquerque, NM 87185
1	Director Sandia National Laboratories Combustion Research Facility ATTN: R. Carling Livermore, CA 94551-0469
1	Director Sandia National Laboratories ATTN: 8741, G. A. Beneditti P.O. Box 969 Livermore, CA 94551-0969
2	Director Lawrence Livermore National Laboratory ATTN: L-355, A. Buckingham M. Finger P.O. Box 808 Livermore, CA 94550-0622
2	Director Los Alamos Scientific Lab ATTN: T3/D. Butler M. Division/B. Craig P.O. Box 1663 Los Alamos, NM 87544
1	Battelle ATTN: TWSTIAC V. Levin 505 King Avenue Columbus, OH 43201-2693
1	Battelle PNL ATTN: M.C.C. Bampton P.O. Box 999 Richland, WA 99352

No. of Copies	Organization
1	Institute of Gas Technology ATTN: D. Gidaspow 3424 S. State Street Chicago, IL 60616-3896
1	Institute for Advanced Technology ATTN: T.M. Kiehne The University of Texas of Austin 4030-2 W. Braker Lane Austin, TX 78759-5329
2	CPIA - JHU ATTN: H. J. Hoffman T. Christian 10630 Little Patuxent Parkway Suite 202 Columbia, MD 21044-3200
1	Brigham Young University Department of Chemical Engineering ATTN: M. Beckstead Provo, UT 84601
1	Jet Propulsion Laboratory California Institute of Technology ATTN: L.D. Strand, MS 125/224 4800 Oak Grove Drive Pasadena, CA 91109
1	California Institute of Technology 204 Karman Lab Main Stop 301-46 ATTN: F.E.C. Culick 1201 E. California Street Pasadena, CA 91109
3	Georgia Institute of Technology School of Aerospace Engineering ATTN: B.T. Zim E. Price W.C. Strahle Atlanta, GA 30332
1	Massachusetts Institute of Technology Department of Mechanical Engineering ATTN: T. Toong 77 Massachusetts Avenue Cambridge, MA 02139-4307
2	University of Illinois Department of Mechanical/Industry Engineering ATTN: H. Krier R. Beddini 144 MEB; 1206 N. Green St. Urbana, IL 61801-2978
1	University of Massachusetts Department of Mechanical Engineering ATTN: K. Jakus Amherst, MA 01002-0014
1	University of Minnesota Department of Mechanical Engineering ATTN: E. Fletcher Minneapolis, MN 55414-3368
3	Pennsylvania State University Department of Mechanical Engineering ATTN: V. Yang K. Kuo C. Merkle University Park, PA 16802-7501
1	Rensselaer Polytechnic Institute Department of Mathematics Troy, NY 12181
1	Stevens Institute of Technology Davidson Laboratory ATTN: R. McAlevy III Castle Point Station Hoboken, NJ 07030-5907
1	Rutgers University Department of Mechanical and Aerospace Engineering ATTN: S. Temkin University Heights Campus New Brunswick, NJ 08903
1	University of Southern California Mechanical Engineering Department ATTN: OHE200, M. Gerstein Los Angeles, CA 90089-5199

No. of Copies	Organization
1	University of Utah Department of Chemical Engineering ATTN: A. Baer Salt Lake City, UT 84112-1194
1	Washington State University Department of Mechanical Engineering ATTN: C.T. Crowe Pullman, WA 99163-5201
1	AFELM, The Rand Corporation ATTN: Library D 1700 Main Street Santa Monica, CA 90401-3297
1	Arrow Technology Associates, Inc. ATTN: W. Hathaway P.O. Box 4218 South Burlington, VT 05401-0042
3	AAI Corporation ATTN: J. Hebert J. Frankle D. Cleveland P.O. Box 126 Hunt Valley, MD 21030-0126
2	Alliant Techsystems, Inc. ATTN: R.E. Tompkins J. Kennedy 7225 Northland Dr. Brooklyn Park, MN 55428
1	Textron ATTN: A. Patrick 2385 Revere Beach Parkway Everett, MA 02149-5900
1	General Applied Sciences Lab ATTN: J. Erdos 77 Raynor Ave. Ronkonkama, NY 11779-6649
1	General Electric Company Tactical System Department ATTN: J. Mandzy 100 Plastics Ave. Pittsfield, MA 01201-3698
1	IITRI ATTN: M.J. Klein 10 W. 35th Street Chicago, IL 60616-3799

No. of Copies	Organization
4	Hercules, Inc. Radford Army Ammunition Plant ATTN: L. Gizzi D.A. Worrell W.J. Worrell C. Chandler Radford, VA 24141-0299
2	Hercules, Inc. Allegheny Ballistics Laboratory ATTN: William B. Walkup Thomas F. Farabaugh P.O. Box 210 Rocket Center, WV 26726
1	Hercules, Inc. Aerospace ATTN: R. Cartwright 100 Howard Blvd. Kenville, NJ 07847
1	Hercules, Inc. Hercules Plaza ATTN: B.M. Riggleman Wilmington, DE 19894
1	MBR Research Inc. ATTN: Dr. Moshe Ben-Reuven 601 Ewing St., Suite C-22 Princeton, NJ 08540
1	Olin Corporation Badger Army Ammunition Plant ATTN: F.E. Wolf Baraboo, WI 53913
3	Olin Ordnance ATTN: E.J. Kirschke A.F. Gonzalez D.W. Worthington P.O. Box 222 St. Marks, FL 32355-0222
1	Olin Ordnance ATTN: H.A. McElroy 10101 9th Street, North St. Petersburg, FL 33716
1	Paul Gough Associates, Inc. ATTN: P.S. Gough 1048 South St. Portsmouth, NH 03801-5423

No. of Copies	Organization
1	Physics International Library ATTN: H. Wayne Wampler P.O. Box 5010 San Leandro, CA 94577-0599
2	Princeton Combustion Research Laboratories, Inc. ATTN: N. Mer N.A. Messina Princeton Corporate Plaza 11 Deerpark Dr., Bldg IV, Suite 119 Monmouth Junction, NJ 08852
3	Rockwell International Rocketdyne Division ATTN: BA08, J. Flanagan J. Gray R.B. Edelman 6633 Canoga Avenue Canoga Park, CA 91303-2703
2	Rockwell International Science Center ATTN: Dr. S. Chakravarthy Dr. S. Palaniswamy 1049 Camino Dos Rios P.O. Box 1085 Thousand Oaks, CA 91360
1	Science Applications International Corp. ATTN: M. Palmer 2109 Air Park Rd. Albuquerque, NM 87106
1	Southwest Research Institute ATTN: J.P. Riegel 6220 Culebra Road P.O. Drawer 28510 San Antonio, TX 78228-0510
1	Sverdrup Technology, Inc. ATTN: Dr. John Deur 2001 Aerospace Parkway Brook Park, OH 44142
3	Thiokol Corporation Elkton Division ATTN: R. Willer R. Biddle Tech Library P.O. Box 241 Elkton, MD 21921-0241
1	Veritay Technology, Inc. ATTN: E. Fisher 4845 Millersport Hwy. East Amherst, NY 14501-0305
1	Universal Propulsion Company ATTN: H.J. McSpadden 25401 North Central Ave. Phoenix, AZ 85027-7837
1	SRI International Propulsion Sciences Division ATTN: Tech Library 333 Ravenwood Avenue Menlo Park, CA 94025-3493
	Aberdeen Proving Ground
1	Cdr, USACSTA ATTN: STECS-PO/R. Hendricksen

This Laboratory undertakes a continuing effort to improve the quality of the reports it publishes. Your comments/answers to the items/questions below will aid us in our efforts.

1. ARL Report Number ARL-CR-68 Date of Report October 1993

2. Date Report Received _____

3. Does this report satisfy a need? (Comment on purpose, related project, or other area of interest for which the report will be used.) _____

4. Specifically, how is the report being used? (Information source, design data, procedure, source of ideas, etc.) _____

5. Has the information in this report led to any quantitative savings as far as man-hours or dollars saved, operating costs avoided, or efficiencies achieved, etc? If so, please elaborate. _____

6. General Comments. What do you think should be changed to improve future reports? (Indicate changes to organization, technical content, format, etc.) _____

CURRENT ADDRESS

_____
Organization

_____
Name

_____
Street or P.O. Box No.

_____
City, State, Zip Code

7. If indicating a Change of Address or Address Correction, please provide the Current or Correct address above and the Old or Incorrect address below.

OLD ADDRESS

_____
Organization

_____
Name

_____
Street or P.O. Box No.

_____
City, State, Zip Code

(Remove this sheet, fold as indicated, tape closed, and mail.)
(DO NOT STAPLE)

DEPARTMENT OF THE ARMY

OFFICIAL BUSINESS

BUSINESS REPLY MAIL
FIRST CLASS PERMIT No 0001, APG, MD

Postage will be paid by addressee

Director
U.S. Army Research Laboratory
ATTN: AMSRL-OP-CI-B (Tech Lib)
Aberdeen Proving Ground, MD 21005-5066

NO POSTAGE
NECESSARY
IF MAILED
IN THE
UNITED STATES